JBIC Journal of Biological Inorganic Chemistry
https://doi.org/10.1007/s00775-019-01651-8

ORIGINAL PAPER

Efficient hydrolytic cleavage of DNA and antiproliferative effect on human cancer cells by two dinuclear Cu(II) complexes containing a carbohydrazone ligand and 1,10-phenanthroline as a coligand

Sidhali U. Parsekar[1] · Manohar Singh[2] · Durga P. Mishra[2] · P. K. Sudhadevi Antharjanam[3] · Aditya P. Koley[4] · Manjuri Kumar[1]

Received: 28 December 2018 / Accepted: 29 January 2019

Abstract

We report the synthesis, crystal structures and biological activities of two dinuclear Cu(II) complexes [Cu(*o*-phen)LCu(OAc)] (**1**) and [Cu(*o*-phen)LCu(*o*-phen)](OAc) (**2**), where *o*-phen = 1,10-phenanthroline, H_3L = *o*-$HOC_6H_4C(H)$=N–NH–C(OH)=N–N=C(H)–C_6H_4OH-*o*, and OAc=CH_3COO^-. Both compounds display strong and broad X-band EPR spectra at RT in their powder state confirming that these are paramagnetic. The intercalative DNA binding of the compounds as revealed from spectrophotometric studies was found to be consistent with the results of fluorescence spectroscopic studies for ethidium bromide displacement assay as well as enhanced viscosity of DNA in the presence of these compounds. The compounds effectively catalyze hydrolytic cleavage of supercoiled *pUC19* DNA and show remarkable cytotoxicity toward human lung cancer A549 cell line (IC_{50} values are 4.34 and 8.46 μM for **1** and **2**, respectively) and breast cancer MCF7 cell line (IC_{50} values are 6.50 and 8.68 μM for **1** and **2**, respectively) and are found to be relatively less toxic toward keratinocyte HaCaT normal cell line (IC_{50} values are 11.19 and 16.01 μM for **1** and **2**, respectively). Annexin-V/PI dual staining results analyzed by flow cytometry strongly suggest the induction of apoptotic pathway for the anticancer activity of these complexes. Flow cytometry experiment for cell cycle analysis showed considerable increase in the G2/M phase in both A549 and MCF7 cell lines by these two compounds. On the other hand, compounds **1** and **2** activate reactive oxygen species (ROS) level in A549 cells, but act as scavengers or inhibitors of ROS in MCF7 cell line as analyzed by DCFDA staining using flow cytometry.

Electronic supplementary material The online version of this article (https://doi.org/10.1007/s00775-019-01651-8) contains supplementary material, which is available to authorized users.

✉ Aditya P. Koley
koleyap@yahoo.co.in

✉ Manjuri Kumar
manjuri@goa.bits-pilani.ac.in

[1] Department of Chemical Engineering, Birla Institute of Technology and Science-Pilani, K.K. Birla Goa Campus, Zuarinagar, Goa 403726, India

[2] Cell Death Research Laboratory, Endocrinology Division, CSIR-Central Drug Research Institute, Lucknow 226031, India

[3] Sophisticated Analytical Instrument Facility, Indian Institute of Technology-Madras, Chennai 600036, India

[4] Department of Chemistry, Birla Institute of Technology and Science-Pilani, K.K. Birla Goa Campus, Zuarinagar, Goa 403726, India

Published online: 18 March 2019

Graphical abstract

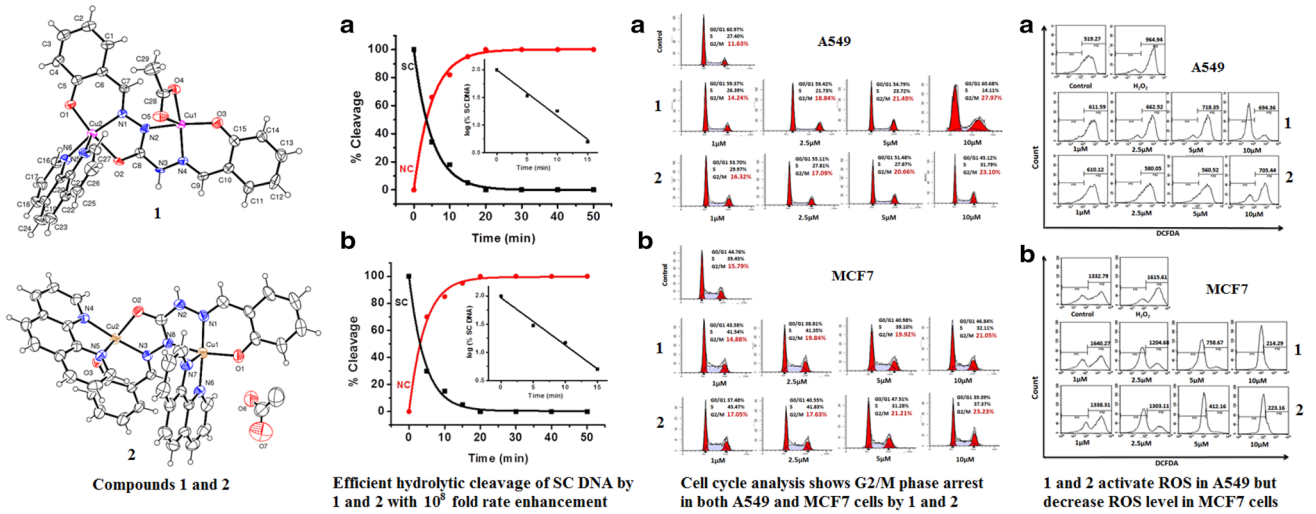

Two dinuclear Cu(II) complexes exhibit efficient hydrolytic cleavage of DNA and display remarkable cytotoxicity against human lung cancer A549 and breast cancer MCF7cells. The ROS level in A549 cells is activated, but the ROS level in MCF7 cells is decreased in the presence of these complexes. Cell cycle analysis by flow cytometry shows G2/M phase arrest in both these cell lines.

Keywords Dinuclear Cu(II) complex · EPR and electronic spectra · DNA binding and cleavage · MTT assay · Cytotoxicity and anticancer activity · Cell cycle analysis

Introduction

Studies involving DNA binding property, nucleic acid cleavage activity and cell cytotoxicity for the metal complexes, Cu(II) complexes in particular due to their biocompatibility and endogeneity have gained momentum in the past two decades to find new metallodrugs that may serve as anticancer agents [1–22]. Many copper(II) complexes cleave DNA in the presence of hydrogen peroxide or ascorbic acid [23–28], but some copper(II) complexes are capable of bringing about hydrolytic cleavage in the absence of any external reagent or light [29–39] in spite of the great stability of the phosphodiester bond in DNA ($k = 3.6 \times 10^{-8}$ h^{-1} for unhydrolyzed ds-DNA) [33, 37]. Since hydrolytic cleavage involves the hydrolysis of the phosphodiester bond, its great stability is a major concern in hydrolytic cleavage. Therefore, there is a necessity of nucleophilic activation for enormous enhancement of the hydrolysis rate to bring about hydrolytic cleavage. Thus, it is a difficult task to find or synthesize a suitable metallodrug that is capable of cleaving DNA hydrolytically under physiological conditions [29–40]. We have synthesized two dinuclear Cu(II) compounds capable of efficient hydrolytic cleavage of supercoiled *pUC19* DNA and also possess remarkable cytotoxicity toward human lung cancer A549 and breast cancer MCF7 cell lines, but less toxic toward keratinocyte HaCaT normal cell line. Here, we present the synthesis, characterization using ESI–MS, IR, UV–visible, EPR, and X-ray crystal structures and the biological activities of these two closely related dinuclear Cu(II) compounds containing the enol form of the Schiff base ligand 1,5-bis(salicylidene)carbohydrazide, but differing in the types of coligand in the two Cu(II) sites. It is to be noted here that we have reported [41] the synthesis and some biological properties such as DNA binding using UV–Vis spectroscopy, cytotoxicity using MTT assay and apoptosis using AO/PI dual staining method for compound **1**, along with the corresponding heterodinuclear Zn(II)–Cu(II) compound (**3**); however, we could not get a single crystal at that time to structurally characterize it. Herein, we confirm its structure by X-ray crystallography along with that of compound **2**, and studied the hydrolytic DNA cleavage. Also, to compare the cytotoxicity and cell cycle analysis for **1** and **2** using human A549 and MCF7 cancer cell lines, we have carried out again the MTT assay for **1** along with that of **2**, as well as studied their apoptosis using Annexin-V and PI double staining and cell cycle analysis using flow cytometry under identical experimental conditions to obtain the exact differences in the biological properties of these two closely related homodinuclear complexes possessing only one *o*-phen coligand in the first Cu(II) site and an acetate in the second Cu(II) site of **1** versus two *o*-phen coligands, one each in both the Cu(II) sites of **2**.

Materials and methods

Materials

Carbohydrazide and salicylaldehyde were obtained from Aldrich. Calf thymus DNA was obtained from Sigma. *N*,*N*-dimethylformamide (DMF, GR), absolute ethanol, methanol (GR), DMSO, 1,10-phenanthroline monohydrate, and $Cu(OAc)_2{\cdot}H_2O$ (GR) were obtained from Merck. Supercoiled (SC) plasmid pUC19 DNA was purchased from Genetix Biotech. All other chemicals were of reagent grades.

Physical measurements

Microanalyses (C, H, N) were performed in a Perkin-Elmer 240C elemental analyzer. Mass spectra were recorded on a PerkinElmer (USA) Flexer SQ 300 MS Mass Spectrometer operating in ESI mode. Infrared spectra were recorded with a Shimadzu IR Affinity-1 FT-IR spectrometer using KBr pellet. Electronic spectra were recorded on a Jasco V-570 UV/VIS/NIR spectrophotometer using a pair of matched quartz cell of path length 1 cm. Electron paramagnetic resonance (EPR) spectra were recorded on a JEOL, Japan Model: JES-FA200 ESR spectrometer with X and Q band. Fluorescence measurements were performed using a Jasco spectrofluorometer model FP-8500.

Syntheses

Preparation of 1,5-bis(salicylidene)carbohydrazide, (o-$HOC_6H_4CH{=}NNH)_2C{=}O$ (H_3L)

This compound was prepared by the reported method of Koley et al. [41]. To a stirring solution of carbohydrazide (5 mmol) dissolved in 30 mL of absolute ethanol, salicylaldehyde (10 mmol) was added dropwise at RT and the reaction mixture was stirred at RT for 2 h while a white compound separated. This was filtered through a G-3 crucible and the pale white solid was washed well with ethanol and air dried. This compound was recrystallized from methanol–ethanol (1:1). Yield 70%; mp 226 °C. Anal. Calc. for $C_{15}H_{14}N_4O_3$: C, 60.40; H, 4.73; N, 18.78. Found: C, 60.57; H, 4.76; N, 18.81%.

Preparation of [Cu(o-phen)LCu(OAc)] (**1**)

This compound was also prepared following the method reported by Koley et al. [41]. In brief, a cold (~ 5°C) solution of 1,10-phenanthroline monohydrate (0.2 g, 0.001 mol) and $Cu(OAc)_2{\cdot}H_2O$ (0.2 g, 0.001 mol) in methanol (30 mL) was very slowly added to a solution of 1,5-bis(salicylidene)carbohydrazide (0.298 g, 0.001 mol) in 50 mL of methanol during 30 min, while the reaction mixture turned bright green. This was stirred at RT for 3 h, then a solution of $Cu(OAc)_2{\cdot}H_2O$ (0.2 g, 0.001 mol) dissolved in methanol (20 mL) was slowly added to this bright green reaction mixture when the solution turned dark green and a dark green compound started separating. This solution was stirred at RT for another 20 h and the dark green compound was filtered through a G-4 crucible, and the mother filtrate was collected. The compound in the crucible was washed well with methanol and air dried, then washed thoroughly with water followed by methanol and dried in vacuo. Yield: 80%. Anal. Calc. for $C_{29}H_{22}N_6O_5Cu_2$: C, 52.65; H, 3.35; N, 12.70. Found: C, 52.55; H, 3.37; N, 12.71%. ESI–MS in DMSO: *m/z* 683.82 $[M+Na]^+$ and *m/z* 701.77 $[M+K+H]^+$.

A part of the mother filtrate was collected in a long tube and left in air for very slow evaporation. Green crystals suitable for X-ray diffraction were obtained within 30 days. We have characterized this compound by X-ray crystal structure (vide infra). These crystals lose their solvent of crystallization (both methanol and water) and become amorphous on long standing at RT or in vacuum.

Preparation of [Cu(o-phen)LCu(o-phen)](OAc) (**2**)

1,10-Phenanthroline monohydrate (0.398 g, 0.002 mol) in 20 mL of methanol was slowly added to a solution of $Cu(OAc)_2{\cdot}H_2O$ (0.398 g, 0.002 mol) dissolved in methanol (20 mL) and the solution was stirred at RT for 30 min and stored at 4 °C. Then this cold blue solution was slowly added to a solution of 1,5-bis(salicylidene)carbohydrazide (0.298 g, 0.001 mol) in 50 mL of methanol during 30 min, while the reaction mixture turned dark green. This was stirred for 20 h at RT and the dark green compound was filtered through a G-4 crucible and the dark green solid was washed very well with methanol and air dried. Then the compound was washed with water and finally washed again with methanol and dried in vacuo. Anal. Calc. for $C_{41}H_{30}N_8O_5Cu_2$: C, 58.44; H, 3.59; N, 13.30. Found: C, 58.49; H, 3.59; N, 13.37%. ESI–MS in CH_3CN: *m/z* 843.7 $[M+2H]^+$ and *m/z* 865.5 $[M+Na+H]^+$.

A saturated methanol solution of this green compound was collected in a 5 mL Corning tube that was placed inside a 15 mL Corning tube containing ~ 2 mL toluene and was covered with a cap and left for slow evaporation at RT when blue crystals were obtained within 30 days and were used for X-ray crystallography. It was noted that on long standing (or in vacuum), these crystals also lose their solvent of crystallization and become amorphous.

X-ray crystallography

[Cu(*o*-phen)LCu(OAc)]$_2$·½CH_3OH·½H_2O

X-ray data collection was performed with Bruker AXS Kappa Apex III CMOS Diffractometer equipped with graphite monochromated Mo (Kα) ($\lambda = 0.71073$ Å) radiation. The automatic cell determination routine, with 24 frames at two different orientations of the detector, was employed to collect reflections for unit cell determination. Further, intensity data for structure determination were collected through an optimized strategy which gave an average fourfold redundancy. The program APEX23-SAINT [42] was used for integrating the frames. Fourfold redundancy per reflection was utilized for achieving good multi-scan absorption correction using the program SADABS [42]. The structure was solved by SHELXT-2014 [43] and refined by full-matrix least-squares techniques using SHELXL-2014, [43] computer program. Molecular graphics were drawn using ORTEP3 [44]. Hydrogens on all carbon atoms were fixed at calculated positions and refined as riding model with C–H = 0.93 Å, (C–H = 0.96 Å for CH_3) Uiso(H) = 1.2Ueq(C) (Uiso(H) = 1.5Ueq(C) for CH_3), whereas hydrogens on nitrogen were fixed from the difference electron density peaks and allowed to refine freely. Since methanol and water solvents are disordered, its site occupancy is constrained at 0.5. Also, the positions of hydrogen on these solvents could not be located and refined satisfactorily and hence ignored. The crystal data belong to a non-merohedrally twinned crystal. The twin law [− 1 0 0, 0 − 1 0.466, 0 0 1] was identified by TwinRotMat program and is used for the generation of HKL5 reflection format which was used for refinement. The percentage of twin is given by a batch-scale factor (BASF) of 0.14.

[Cu(*o*-phen)LCu(*o*-phen)](OAc)·H_2O

X-ray data collection was performed with Bruker AXS Kappa Apex III CMOS dual source diffractometer with Cu (Kα) ($\lambda = 1.54178$ Å) radiation. The automatic cell determination routine, with 40 frames at two different orientations of the detector, was employed to collect reflections for unit cell determination. Further, intensity data for structure determination were collected through an optimized strategy which gave an average fourfold redundancy. The program APEX3-SAINT [42] was used for integrating the frames. Fourfold redundancy per reflection was utilized for achieving good multi-scan absorption correction using the program SADABS [42]. The structure was solved by SHELXT-2014 [43] and refined by full-matrix least-squares techniques using SHELXL-2014 [43] computer program. Molecular graphics were drawn using ORTEP3 [44]. All hydrogens were fixed at calculated positions and refined as riding model with C–H or N–H 0.93 Å, (C–H = 0.96 Å for CH_3) Uiso(H) = 1.2Ueq(C) (Uiso(H) = 1.5Ueq(C) for CH_3 and N–H). The acetate anion is triply disordered with site occupancies in the ratio of 42:24:34. Hydrogens on disordered solvent molecules could not be located. Crystal data and structure refinement for **1** and **2** are presented in Table 1.

DNA binding experiments

Absorption spectral studies

Absorption titrations were performed by adding incremental amounts of calf thymus DNA (CT-DNA) to a complex solution having concentration of 5×10^{-5} M in 10 mM Tris–HCl buffer at pH 7.4. The concentration of CT-DNA was calculated from the absorbance at 260 nm with the molar extinction coefficient for CT-DNA as 6600 M^{-1} cm^{-1} at 260 nm. After every incremental addition of DNA, the reaction mixture was allowed to equilibrate for 2 min at room temperature after which the absorption spectra was recorded. The experimental data were used to calculate the intrinsic binding constant K_b.

Viscosity measurements

Viscosity measurements were carried using CT-DNA (100 µM) with increasing concentrations (0–100 µM) of the complexes **1** and **2** using Ostwald viscometer. Viscosity values were calculated from the flow time of buffer alone (t_0) and flow time of each sample (t) using the equation $\eta = (t - t_0)/t_0$. Data were presented by plotting values of relative viscosity $(\eta/\eta_0)^{1/3}$ against [complex]/[DNA], where η is the viscosity of DNA in the presence of complex and η_0 is the viscosity of DNA alone.

Competitive DNA binding fluorescence measurements

The competitive binding studies using ethidium bromide (EB)-bound CT-DNA was investigated using fluorescent spectrometry. The experiments were carried out by adding incremental amounts of complexes **1** and **2** into EB–DNA solution (2 µM EB and 50 µM CT-DNA) in 10 mM Tris HCl buffer (pH 7.9). The solutions were incubated at room temperature for 5 min to fully react, prior to recording the spectra. The effect of addition of increasing amounts of **1** and **2** to the EB–DNA complex was monitored by recording the variation of fluorescence emission spectra with excitation at 510 nm and emission at 597 nm. The behavior was analyzed through the Stern–Volmer equation and the apparent binding constant (K_{app}) was calculated.

Table 1 Crystal data[a] and structure refinement for **1** and **2**

Identification code	Compound **1**	Compound **2**
Empirical formula	$C_{117}\,H_{88}\,Cu_8\,N_{24}\,O_{22}$	$C_{41}\,H_{32}\,Cu_2\,N_8\,O_6$
Formula weight	2690.43	859.82
Temperature	296(2) K	296(2) K
Wavelength	0.71073 Å	1.54178 Å
Crystal system	Triclinic	Triclinic
Space group	P-1	P-1
Unit cell dimensions	$a = 12.4593(2)$ Å	$a = 12.0174(7)$ Å
	$b = 16.0360(2)$ Å	$b = 12.1041(6)$ Å
	$c = 16.0585(3)$ Å	$c = 14.5463(7)$ Å
	$\alpha = 76.521(6)°$	$\alpha = 107.890(3)°$
	$\beta = 89.935(7)°$	$\beta = 97.769(4)°$
	$\gamma = 67.478(6)°$	$\gamma = 107.645(4)°$
Volume	2868.20(16) $Å^3$	1857.06(18) $Å^3$
Z	1	2
Density (calculated)	1.558 mg/m^3	1.538 mg/m^3
Absorption coefficient	1.535 mm^{-1}	1.923 mm^{-1}
$F(000)$	1366	880
Crystal size	$0.100 \times 0.100 \times 0.050$ mm^3	$0.100 \times 0.100 \times 0.050$ mm^3
Theta range for data collection	2.678°–21.910°	3.299°–66.992°
Index ranges	$-12 \le h \le 12, -16 \le k \le 16, -16 \le l \le 16$	$-13 \le h \le 14, -14 \le k \le 14, -17 \le l \le 17$
Reflections collected	33,612	48,548
Independent reflections	33,612 [$R(\text{int}) = ?$]	6616 [$R(\text{int}) = 0.2148$]
Completeness to theta	(= 21.910°) 98.5%	(= 66.992°) 99.9%
Absorption correction	Semi-empirical from equivalents	Semi-empirical from equivalents
Max. and min. transmission	0.7457 and 0.5487	0.75 and 0.63
Refinement method	Full-matrix least-squares on F^2	Full-matrix least-squares on F^2
Data/restraints/parameters	33,612/64/789	6616/250/600
Goodness-of-fit on F^2	1.047	1.022
Final R indices [$I > 2\text{sigma}(I)$]	$R1 = 0.0823$, $wR2 = 0.2295$	$R1 = 0.0785$, $wR2 = 0.1802$
R indices (all data)	$R1 = 0.1249$, $wR2 = 0.2627$	$R1 = 0.1550$, $wR2 = 0.2245$
Extinction coefficient	n/a	0.0004(2)
Largest diff. peak and hole	1.478 and −0.816 e $Å^{-3}$	0.623 and −0.531 e $Å^{-3}$

[a]Crystallographic data for the structural analysis have been deposited with the Cambridge Crystallographic Data Center; numbers are CCDC 1887320 for compound **1** and CCDC 1887321 for compound **2**, respectively

DNA cleavage experiments

The interaction of the complexes **1** and **2** with supercoiled pUC19 DNA was studied using agarose gel electrophoresis. The cleavage of pUC19 DNA was accomplished by treating SC plasmid pUC19 DNA (200 ng) with different concentrations of complexes **1** and **2** in 50 mM Tris–HCl buffer (pH 8.0), the samples were incubated for 3 h at 37 °C in dark, after which a loading buffer containing 25% bromophenol blue, 0.25% xylene cyanol and 30% glycerol was added, electrophoresis was performed at 60 V for 1.5 h and analyzed for cleaved products. The gel was stained with 0.5 µg/mL ethidium bromide and viewed under UV light. The bands originating from SC (form I) and NC (form II) in hydrolytic DNA cleavage experiments were quantified using image J. The ability of the complexes to convert the supercoiled (SC, form I) to nicked circular (NC, form II) DNA was used to measure the cleavage efficiency.

Oxidative DNA cleavage by the complexes was studied by performing reactions in dark using hydrogen peroxide (0.1 mM) as the oxidizing agent in the absence and presence of the complex (0–25 µM). The solutions were incubated at 37 °C for 1 h, subjected to electrophoresis and analyzed for DNA cleaved products. For mechanistic investigations, experiments were also conducted in the presence of radical scavengers such as DMSO (2 µL), a hydroxyl radical scavenger, and NaN_3 (100 µM), a singlet oxygen quencher, which were added to pUC19 DNA prior to the addition of complex.

To ensure that the copper complexes **1** and **2** as a whole are responsible for cleavage of DNA, control experiments were performed with $Cu(OAc)_2{\cdot}H_2O$ (500 µM), free ligands 1,5-bis(salicylidene)carbohydrazide (500 µM) and 1,10-phenanthroline monohydrate (500 µM).

For kinetic measurements, the DNA cleavage rate was measured keeping fixed concentrations of DNA (200 ng) and **1** or **2** (200 µM) at 37 °C for different time intervals. The decrease in form I was plotted against time and the data fitted into a single exponential decay curve; thereafter, the hydrolysis rate constant K_{obs} was calculated to determine the rate enhancement in comparison to that of unhydrolyzed rate of ds-DNA.

Cell culture and treatment

Cancer cell lines A549, MCF7 and normal human keratinocyte HaCaT cells were obtained from American Type Culture Collection (ATCC; Manassas, VA, USA). HaCaT and MCF7 cell lines were cultured in DMEM, while A549 cell line was cultured in DMEM F12, supplemented with 10% FBS and antibiotic–antimycotic at 37 °C with 5% CO_2 in a CO_2 incubator. The cells were subcultured after they had reached 70–80% confluence by trypsinization and used for further experimental purpose.

Cell viability assay

Cell viability was assessed by MTT assay according to a previously standardized protocol [45, 46]. Briefly, A549, MCF7 and HaCaT cells (5×10^3 cells/well) were seeded in 96-well plates and treated with 1, 2.5, 5, 10, 15 and 20 µM of compounds **1** and **2** for 24 h. After completion of treatment, cells were incubated with 500 µg/mL MTT (3-(4,5-dimethylthiazol-2-yl)-2-5-diphenyltetrazolium) at 37 °C for 2 h. Culture media were removed and the formazan crystals were dissolved in 100 µL of DMSO. The color intensity was measured in a BMG fluostar Optima plate reader at 450 nm and percentage cell viability was calculated. The cytotoxicity of the free Schiff base ligand and the free coligand 1,10-phenanthroline were also studied using the human lung cancer A549 cell line with different concentrations (0.5 µM, 1.0 µM, 2.5 µM, 5 µM and 10 µM) of these free ligands.

Quantification of apoptosis by Annexin-V and PI double staining

A549 and MCF7 cells were cultured in DMEM media and treated with different concentrations (1, 2.5, 5, 10, 15 and 20 µM) of compounds **1** and **2** for 24 h. Apoptosis was measured by flow cytometry using Annexin-V/PI labeling according to the previously described protocol [45, 46]. Briefly, A549 and MCF7 cells were incubated in 100 µL staining solution (5 µL PI and 3 µL Annexin-V FITC in the 1× binding buffer) for 15 min at room temperature. The volume was made up to 300 µL by 1× binding buffer and apoptosis was measured using flow cytometry FACS caliber and data were analyzed with Modfit software.

Cell cycle analysis

The different phases of cell cycle were analyzed by flow cytometry as in a previously described protocol [45, 46]. A549 and MCF7 cells were cultured in DMEM media and treated with 1 µM, 2.5 µM, 5 µM and 10 µM concentration of compounds **1** and **2** for 24 h. In brief, cells were fixed in 70% ice cold ethanol for 1 h on ice and washed with 1× PBS twice. Fixed cells were incubated in 300 µL staining solution (50 µg/mL propidium iodide and 50 µg/mL RNaseA in 1× PBS for 30 min at room temperature in dark). Specific cell cycle phase arrest was assessed by FACS caliber and data were analyzed with Modfit software.

Reactive oxygen species (ROS) detection assay

The generation of reactive oxygen species (ROS) in A549 and MCF7 cells was detected using ROS-sensitive fluorescent probe 2′,7′-dichlorodihydrofluorescein diacetate (H_2DCFDA). In cells, H_2DCFDA is hydrolyzed by esterases into H_2DCF and further oxidized by ROS to 2′,7′-dichlorodihydrofluorescein (DCF) which exhibits intense green fluorescence. Briefly, the cultured cells were treated with different concentrations (1, 2.5, 5 and 10 µM) of compounds **1** and **2** for 24 h, untreated cells were maintained as control and cells treated with freshly prepared H_2O_2 were used as positive control. After completion of treatment, cells were trypsinized and washed with 1× PBS. Subsequently, the samples were incubated in 10 µM DCFDA for 30 min at room temperature in dark. Cellular reactive oxygen species (ROS) generation was measured by flow cytometry by DCFDA staining at 488 nm excitation and 535 emission laser.

Statistical analysis

All assays with established cell lines were repeated three times. Data are expressed as the mean ± standard deviation and analyzed by one-way analysis with differences considered significant at *<0.05, **<0.01, and ***<0.001 (GraphPad Prism 5).

Results and discussion

Synthesis and characterization

The free Schiff base ligand 1,5-bis(salicylidene)carbohydrazide (A) which is in keto form in the solid [41] can be

in its enol form in solution that can exist either in syn (B) or anti (B′) as shown in Scheme 1. B′ possesses two distinctly different tridentate coordination sites: the first site is characterized by one phenolate O^-, one enolate O^- and one imine N, and the second site is characterized by other phenolate O^-, other imine N and the secondary NH donor atom. Coordination of the ligand in its B′ form in both **1** and **2** is confirmed from the crystal structures of both the compounds (vide infra).

The reaction of $Cu(OAc)_2{\cdot}H_2O$ with 1,5-bis(salicylidene) carbohydrazide (A) in methanol in the presence of 1,10-phenanthroline (*o*-phen) in the ratio of 2:1:1 resulted in the dinuclear Cu(II) complex containing one coordinated *o*-phen coligand to the first Cu(II) center and one acetate coordinated to the second Cu(II) center in compound **1**, and the reaction in the ratio of 2:1:2 yielded compound **2**, both the Cu(II) centers containing one *o*-phen each and one acetate counteranion.

The solubility of the complexes is low in methanol and acetonitrile, but they are readily soluble in DMF and DMSO. The ESI-MS spectra for complexes **1**–**2** have been recorded in the positive-ion mode and the results are presented in Fig. S1 (Supplementary material). Complex **1** showed peaks at *m/z* 683.82 $[M+Na]^+$ and *m/z* 701.77 $[M+K+H]^{+,}$ while compound **2** showed peaks at *m/z* 843.7 $[M+2H]^+$ and *m/z* 865.5 $[M+Na+H]^+$, respectively. Both the compounds display strong X-band EPR at RT in their powder state (Fig. S2, Supplementary material) with *g* values of 2.09 for **1** and 2.10 for **2**, suggesting they are paramagnetic. Also, the presence of forbidden $\Delta Ms = \pm 2$ line around $g \sim 4$ in both of them (Fig. S2, inset) clearly suggests that it results from a dimer Cu–Cu interaction. Based on their physico-chemical properties, elemental analysis, mass spectra and X-band EPR results, the proposed structures of **1**–**2** are shown in Scheme 2.

The IR spectrum of the powder sample of the free ligand 1,5-bis(salicylidene)carbohydrazide (A) clearly shows the ν(C=O) at 1690 cm^{-1} and ν(C=N) at 1625 cm^{-1} (figure not shown), respectively, suggesting it exists in its keto form which was confirmed previously from its crystal structure [41]. The ν(C=O) band at 1690 cm^{-1} is found to be absent in the IR spectra of both **1** and **2**, and the band at 1625 cm^{-1} due to ν(C=N) of the free ligand is shifted to 1605 cm^{-1} in the IR spectra of both the complexes indicating the coordination of the imine N to the metal ion. This is confirmed from the crystal structures of **1** and **2**.

The electronic absorption spectra of both the compounds in DMSO are found to be very similar (Fig. S3, Supplementary material) suggesting their very similar electronic structures. Both the compounds display ligand field transitions around 622 nm, followed by strong LMCT in the visible region apart from other charge transfer transitions in the UV region.

Crystal structures of [Cu(*o*-phen)LCu(OAc)]$_2$·½CH_3OH·½H_2O and [Cu(*o*-phen)LCu(*o*-phen)] (OAc)·H_2O

The structures of the compounds **1** and **2** have been determined by X-ray crystallography. Figure 1 shows the ORTEP representation of the molecule of **1** with 40%

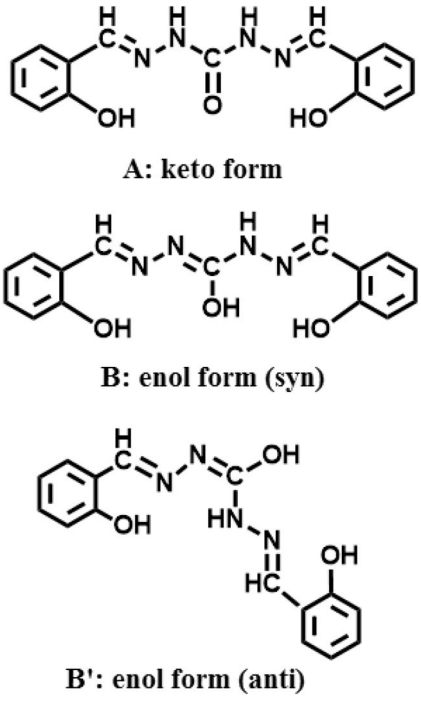

Scheme 1 Proposed structures of the ligand in its keto and enol forms

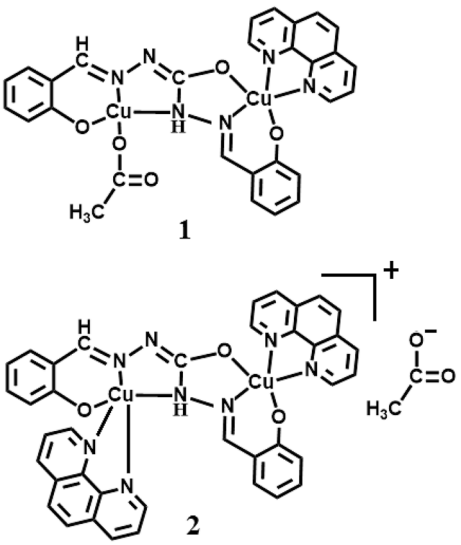

Scheme 2 Proposed structures of the compounds **1**–**2**

probability ellipsoids [44]. The crystal for **1** is indexed in triclinic system with space group P-1 and lattice parameters $a = 12.4593(2)$ Å, $b = 16.0360(2)$ Å, $c = 16.0585(3)$ Å, $\alpha = 76.521(6)°$, $\beta = 89.935(7)°$, $\gamma = 67.478(6)°$.

The asymmetric unit of the crystal contains two crystallographically independent molecules of binuclear copper complex, half molecule of methanol and half molecule of water. The central copper atom shows penta-coordination forming distorted square pyramidal geometry. The unique hexadentate ligand connects two copper atoms with a Cu–Cu distance of 4.75 Å. The acetate anion is co-ordinated to Cu1 and Cu3 through its bidentate binding mode and the 1,10-phenanthroline moiety is co-ordinated to Cu2 and Cu4. The two binuclear copper complexes in the asymmetric unit are held (Fig. 2) together by N(3)-H(3A)…O(10) hydrogen bond interaction with a d(H…A) distance of 1.94(5) Å. In addition to this, the crystal lattice is stabilized by CH…O and CH…π interactions and also by the

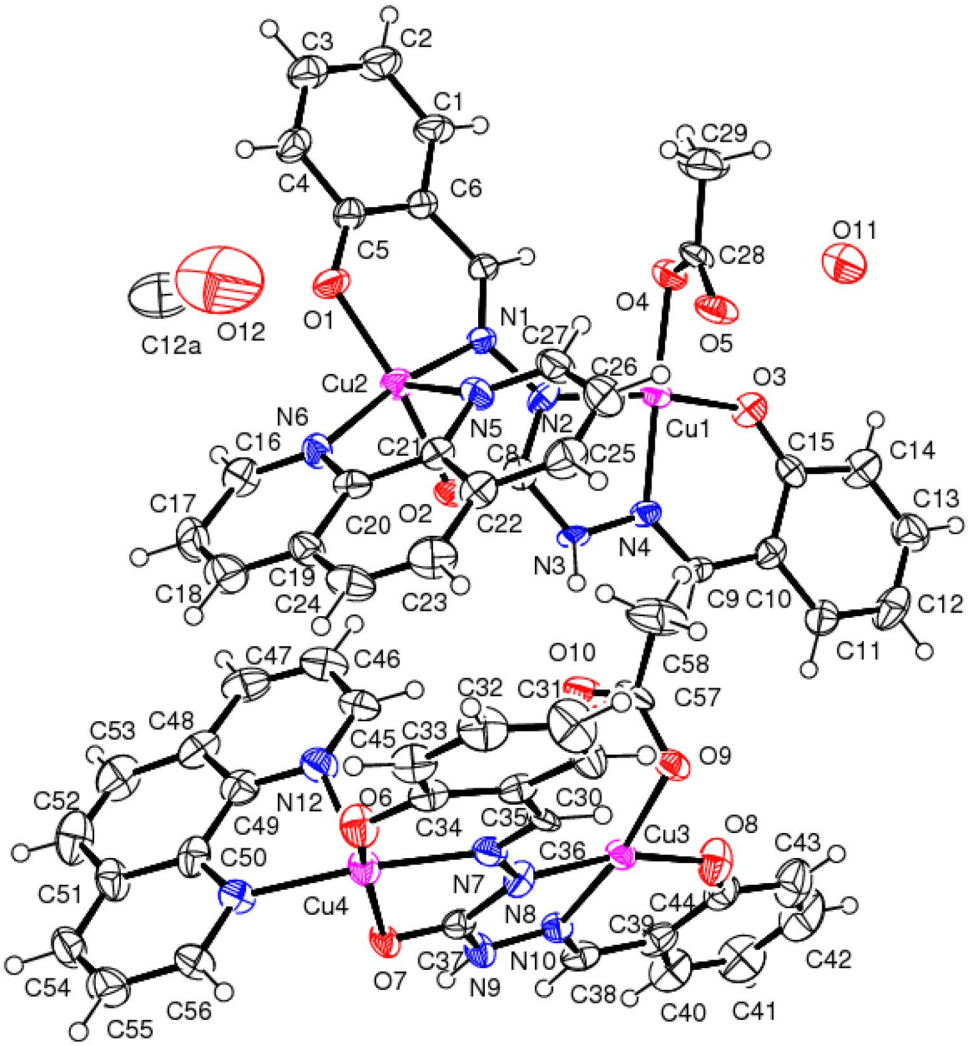

Fig. 1 ORTEP diagram of the compound [Cu(*o*-phen) LCu(OAc)]$_2$·½CH_3OH·½H_2O. Selected bond lengths (Å) and angles (°):N(1)–Cu(2), 1.918(10); N(2)–Cu(1), 1.978(11); N(4)–Cu(1), 1.964(10); N(5)–Cu(2), 2.266(12); N(6)–Cu(2), 1.985(11); N(7)–Cu(4), 1.944(11); N(8)–Cu(3), 1.999(11); N(10)–Cu(3), 1.958(11); N(11)–Cu(4), 1.996(11); N(12)–Cu(4), 2.264(11); O(1)–Cu(2), 1.899(9); O(2)–Cu(2), 2.013(9); O(3)–Cu(1), 1.880(10); O(4)–Cu(1), 1.956(9); O(6)–Cu(4), 1.895(10); O(7)–Cu(4), 2.018(9); O(8)–Cu(3), 1.883(10); O(9)–Cu(3), 1.958(9); O(3)–Cu(1)–O(4), 93.5(4); O(3)–Cu(1)–N(4), 90.9(4); O(4)–Cu(1)–N(4), 169.8(4); O(3)–Cu(1)–N(2), 166.0(5); O(4)–Cu(1)–N(2), 96.7(4); N(4)–Cu(1)–N(2), 80.7(4); O(1)–Cu(2)–N(1), 94.5(4); O(1)–Cu(2)–N(6), 95.3(4); N(1)–Cu(2)–N(6), 169.7(4); O(1)–Cu(2)–O(2), 163.1(4); N(1)–Cu(2)–O(2), 81.5(4); N(6)–Cu(2)–O(2), 88.2(4); O(1)–Cu(2)–N(5), 110.5(4); N(1)–Cu(2)–N(5), 99.3(4); N(6)–Cu(2)–N(5), 80.0(4); O(2)–Cu(2)–N(5), 86.3(4); O(8)–Cu(3)–N(10), 91.2(5); O(8)–Cu(3)–O(9), 93.2(4); N(10)–Cu(3)–O(9), 170.4(4); O(8)–Cu(3)–N(8), 165.5(5); N(10)–Cu(3)–N(8), 80.1(4); O(9)–Cu(3)–N(8), 97.2(4); O(6)–Cu(4)–N(7), 94.5(5); O(6)–Cu(4)–N(11), 95.5(4); N(7)–Cu(4)–N(11), 169.7(5); O(6)–Cu(4)–O(7), 162.7(4); N(7)–Cu(4)–O(7), 81.1(4); N(11)–Cu(4)–O(7), 88.6(4); O(6)–Cu(4)–N(12), 111.4(4); N(7)–Cu(4)–N(12), 99.5(4); N(11)–Cu(4)–N(12), 79.2(4); O(7)–Cu(4)–N(12), 85.9(4)

solvent-mediated hydrogen bond interactions. The overall structure of this compound is found to be similar to that of the compound Zn(*o*-phen)LCu(OAc)·0.5H_2O·0.5CH_3OH we have reported earlier [41].

Figure 3 shows the ORTEP representation of compound **2** with 40% probability ellipsoids [42]. The molecule of **2** crystallizes in triclinic crystal system with space group P-1. The lattice parameters are: $a = 12.0174(7)$ Å, $b = 12.1041(6)$ Å, $c = 14.5463(7)$ Å, $\alpha = 107.890(3)°$, $\beta = 97.769(4)°$, $\gamma = 107.645(4)°$. The asymmetric unit of the crystal contains one binuclear copper complex, one molecule of acetate anion and one molecule of water. The copper atoms show penta-coordination forming distorted square pyramidal geometry. The unique hexadentate ligand connects two copper atoms with a Cu–Cu distance of 4.73 Å. The disordered acetate anion does not show any coordination to metal atoms; instead, it participates in H-bond interaction with the N–H moiety of the hexadentate ligand. Solvent-mediated H-bond interactions hold the binuclear copper complexes together in the crystal lattice (Fig. 4).

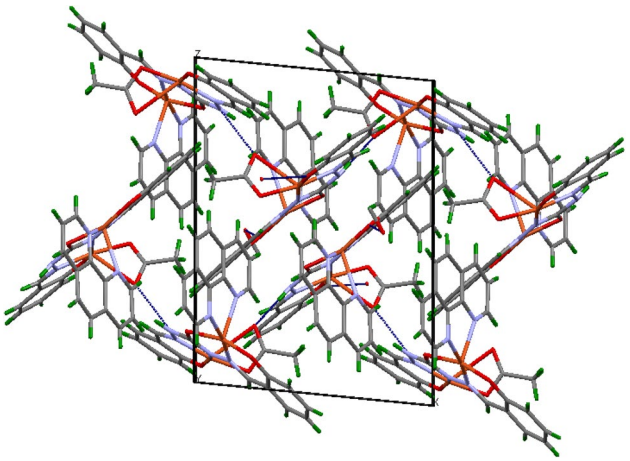

Fig. 2 Packing of the molecules of **1** in the unit cell

DNA binding studies

Absorption spectroscopic studies

The binding affinity of complex **2** toward calf thymus DNA (CT-DNA) has been studied by electronic absorption spectroscopy. In general, the absorption spectra of metal complexes binding to CT-DNA through intercalative mode show decrease in molar absorptivity due to strong stacking interaction between the aromatic chromophore of the ligand and

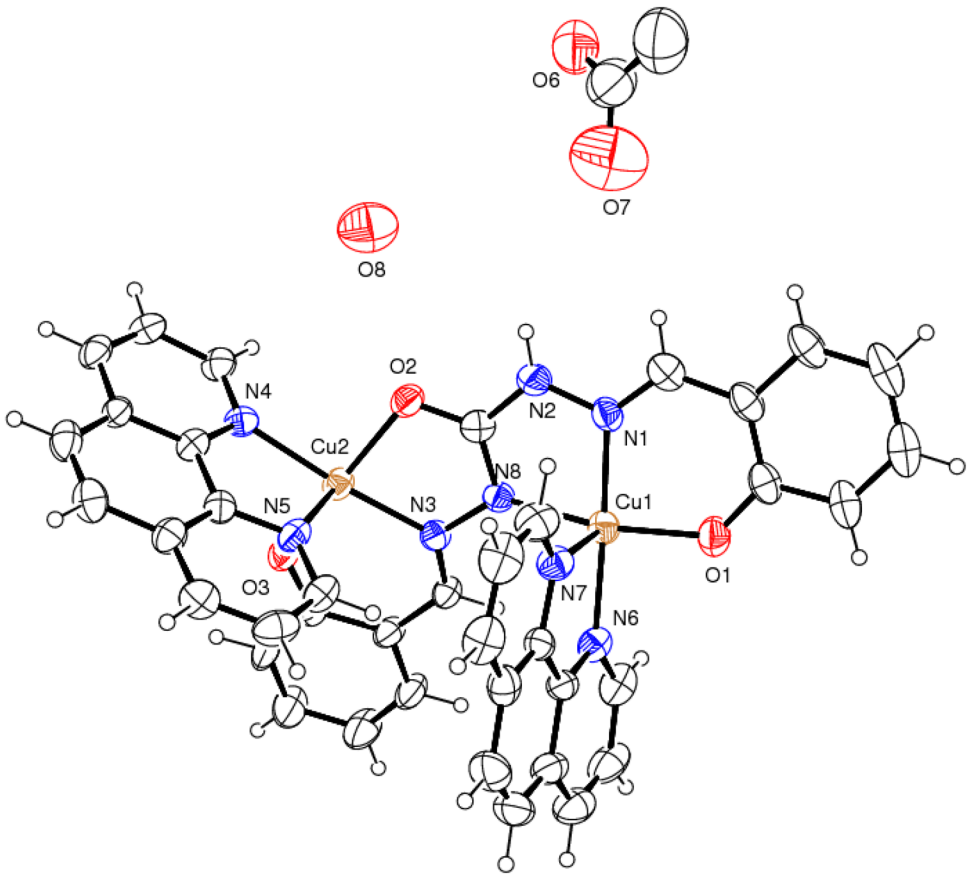

Fig. 3 ORTEP diagram of the compound [Cu(*o*-phen)LCu(*o*-phen)] (OAc)·H_2O. Selected bond lengths (Å) and angles (°):N(1)–Cu(1), 1.948(6); N(3)–Cu(2), 1.936(6); N(4)–Cu(2), 2.024(6); N(5)–Cu(2), 2.306(6); N(6)–Cu(1), 2.021(6); N(7)–Cu(1), 2.326(7); N(8)–Cu(1), 2.005(6); O(1)–Cu(1), 1.901(5); O(2)–Cu(2), 1.959(5); O(3)–Cu(2), 1.902(5); O(1)–Cu(1)–N(8), 162.4(3); N(1)–Cu(1)–N(8), 79.8(2); O(1)–Cu(1)–N(6), 90.0(2); N(1)–Cu(1)–N(6), 174.2(3); N(8)–Cu(1)–N(6), 99.8(2); O(1)–Cu(1)–N(7), 103.1(2); N(1)–Cu(1)–N(7), 97.2(2); N(8)–Cu(1)–N(7), 93.4(2); N(6)–Cu(1)–N(7), 77.0(2); O(3)–Cu(2)–N(3), 93.7(2); O(3)–Cu(2)–O(2), 163.3(2); N(3)–Cu(2)–O(2), 81.4(2); O(3)–Cu(2)–N(4), 92.0(2); N(3)–Cu(2)–N(4), 174.3(2); O(2)–Cu(2)–N(4), 93.0(2); O(3)–Cu(2)–N(5), 95.3(2); N(3)–Cu(2)–N(5), 103.1(2); O(2)–Cu(2)–N(5), 101.3(2); N(4)–Cu(2)–N(5), 76.8(2)

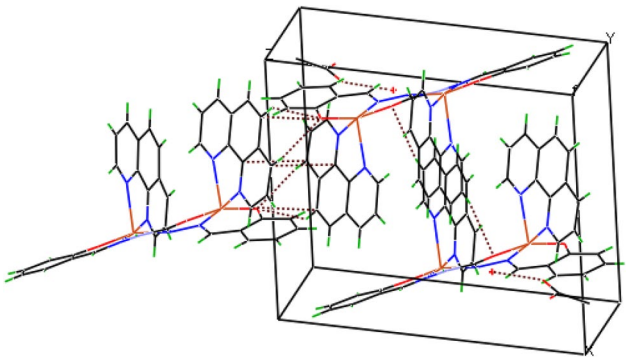

Fig. 4 Packing of the molecules of **2** in the unit cell

the DNA base pairs. The UV–Vis absorption spectrum of compound **2** is significantly perturbed on addition of incremental amounts of CT-DNA (Fig. 5). The absorption band at 396 nm shows hypochromism of 67.3% for **2**. The observed spectroscopic changes thus imply intercalation of **2** into the DNA base stack. A similar result was observed for **1** as we have reported earlier [41]. The intrinsic binding constant (K_b) for the association of **2** with CT-DNA was determined quantitatively using the Eq. (1):

$$\frac{[DNA]}{(\varepsilon_a - \varepsilon_f)} = \frac{[DNA]}{(\varepsilon_b - \varepsilon_f)} + \frac{1}{K_b(\varepsilon_b - \varepsilon_f)}, \quad (1)$$

where [DNA] denotes the concentration of CT-DNA, and the apparent extinction coefficient (ε_a) was obtained by calculating Abs/[complex]. The terms ε_f and ε_b denote the extinction coefficients of free (unbound) and the fully bound complexes, respectively. The binding constant was calculated from the ratio of the slope to the intercept of the plot of [DNA]/($\varepsilon_a - \varepsilon_f$) versus [DNA]. The observed K_b value was found to be 2.86×10^5 M^{-1} for **2** which is slightly higher than that reported (2.63×10^5 M^{-1}) for **1** [41], suggesting that complex **2** has a higher DNA binding affinity than **1**.

Viscosity measurements

As a means to further support the intercalative mode of DNA binding results obtained from spectroscopic analysis, viscosity measurements were carried out to study the effect of increasing concentrations of both **1** and **2** on CT-DNA. A classical intercalative mode of binding causes significant increase in viscosity, because insertion of intercalator causes the base pairs of DNA to separate and unwind resulting in an increase in the overall length of DNA, which increases the viscosity. Based on our observations, the data plotted for the relative viscosity $(\eta/\eta_0)^{1/3}$ against [complex]/[DNA] (Fig. 6) reveal that there is steady increase in viscosity in case of both copper complexes **1** and **2** which confirms the intercalative mode of binding of the copper(II) complexes to CT-DNA. It is to be noted that increase in viscosity is more prominent in **2** than **1** which is found to be in line with spectral studies.

Competitive DNA binding: fluorescence studies

Ethidium bromide (EB) is a planar intercalating dye which emits fluorescence upon binding to calf thymus DNA. We performed ethidium bromide displacement assay to examine the ability of the complexes **1** and **2** to replace EB from the EB–DNA complex. The interaction of complexes **1** and **2** with ethidium bromide-bound CT-DNA in 10 mM Tris–HCl buffer (pH 7.9) was carried out and it was found that the

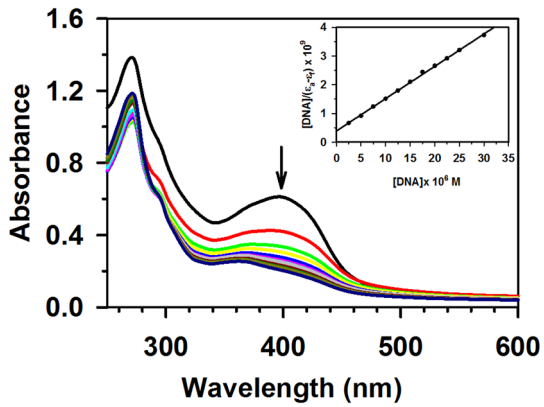

Fig. 5 Change in electronic absorption spectra of **2** [5×10^{-5} M] upon titration with CT-DNA (0–30 μM) dissolved in 10 mM Tris–HCl buffer (pH 7.4). The figure in inset shows the linear fit of [DNA]/($\varepsilon_a - \varepsilon_f$) versus [DNA]. Intrinsic binding constant $K_b = 2.86 \times 10^5$ M^{-1} ($R^2 = 0.99874$ for 11 points)

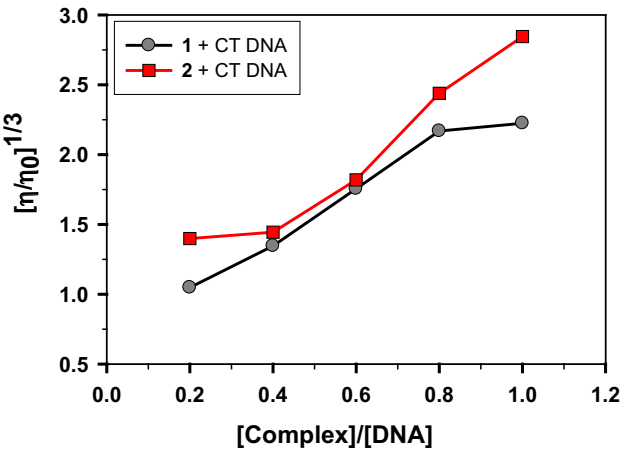

Fig. 6 Effect of increasing amount of **1** and **2** on the relative viscosity of CT-DNA (100 μM) in 10 mM Tris–HCl buffer (pH 7.4) at room temperature

emission band at 597 nm of the EB–DNA system decreased in intensity with increase in complex concentration (Fig. 7). This observation implies that both the complexes have been able to displace EB from EB–DNA complex and such characteristic decrease is observed in DNA interaction by the intercalative mode. The quenching of EB bound to DNA by the copper complexes **1** and **2** is in agreement with the linear Stern–Volmer equation (2) (Fig. 7 inset):

$$\frac{F_o}{F} = 1 + K_{SV}[Q], \tag{2}$$

where F_0 and F are the emission intensities of EB-bound CT-DNA in the absence and presence of the quencher (complex) concentration [Q], respectively, and is the K_{SV} Stern–Volmer quenching constant. The plot of F/F_0 vs. complex concentration at 597 nm was used to calculate the apparent binding constant from 50% quenching using Eq. (3):

$$K_{EB}[EB] = K_{app}[complex]_{50}, \tag{3}$$

where $[complex]_{50}$ is the complex concentration at 50% reduction of the fluorescence intensity of EB-bound CT-DNA, K_{EB} is the binding constant of EB ($K_{EB} = 1.0 \times 10^7\ M^{-1}$) and [EB] is the concentration of ethidium bromide used (2 μM). The calculated apparent binding constant (K_{app}) for the complexes are $1.02 \times 10^6\ M^{-1}$ for complex **1** and $1.43 \times 10^6\ M^{-1}$ for **2**, thus it is observed that K_{app} of **2** > **1,** which shows a similar trend to the K_b values obtained from UV–Vis absorption spectral studies. It is also to be noted that the K_{app} of the complexes **1** and **2** are observed to be tenfold lower than the binding constant of classical intercalator EB ($1 \times 10^7\ M^{-1}$).

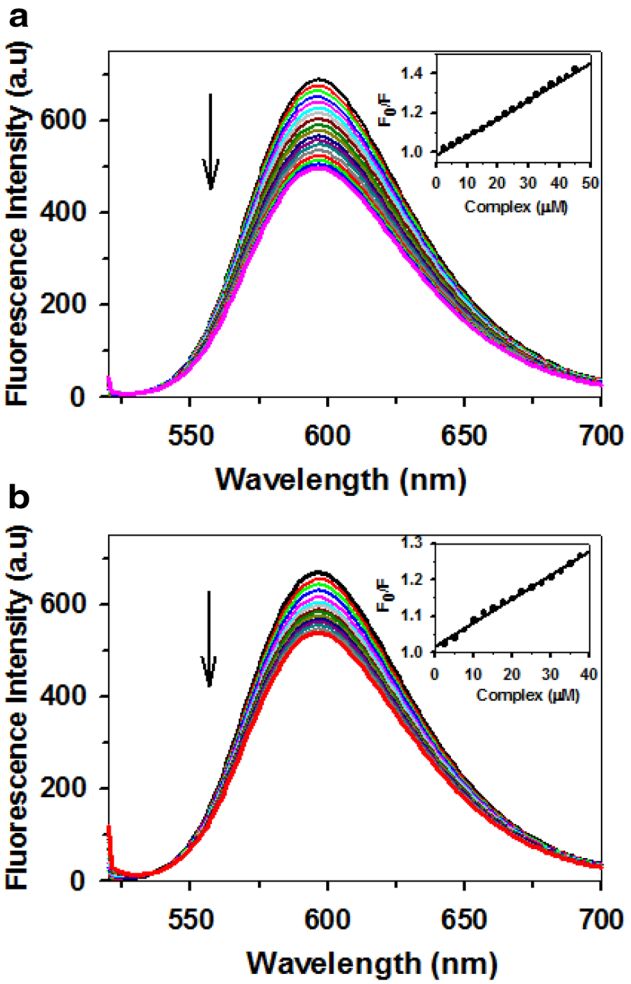

Fig. 7 Effect of the addition of complexes **1** (**a**) and **2** (**b**) on the emission intensity of ethidium bromide-bound CT-DNA at different concentrations in 10 mM Tris–HCl buffer (pH 7.9). $\lambda_{ex} = 510$ nm. The arrow shows the change in fluorescence intensity with increasing complex concentration. The inset shows the linear fit of F_0/F versus [complex]

Cleavage activity with pUC19 DNA

The ability of the complexes **1** and **2** to cleave DNA was assessed by performing gel electrophoresis on supercoiled plasmid DNA pUC19 as the substrate in a medium of 50 mM Tris–HCl buffer (pH 8.0) in the absence of any external additives or light. Both complexes were found to cleave DNA hydrolytically. The distribution of the supercoiled (SC) and nicked forms (NC) in the agarose gel electrophoresis was used to measure the extent of hydrolysis of the phosphodiester bond. At a complex concentration of 30 μM and an incubation time of 3 h, **1** cleaves 19% of SC DNA (Fig. 8a, lane 5), while 90% cleavage is observed for **2** (Fig. 8c, lane 5). Again at 50 μM concentration, **1** cleaves 87% of SC DNA (Fig. 8b, lane 2), while complete cleavage is observed for **2** (Fig. 8d, lane 2). This greater nuclease activity of **2** as compared to **1** can be possibly rationalized on the basis of its higher binding affinity toward CT-DNA as reflected from DNA binding studies.

The nuclease activity of the complexes has also been studied in the presence of H_2O_2. A figure representing oxidative DNA cleavage by complex **2** has been incorporated (Fig. 8e, lanes 1–4), which shows that with increasing concentration (0–25 μM) of complex **2**, supercoiled DNA is gradually converted completely to the nicked form. To elucidate the mechanistic aspects of the chemical-induced DNA cleavage, experiments were conducted in the presence of inhibitors. Oxidative DNA cleavage performed in the presence of DMSO, a known scavenger of hydroxyl ion, showed considerable inhibition of cleavage (Fig. 8e, lane 5); on the other hand, the presence of NaN_3, a singlet oxygen quencher, did not have any considerable effect on the DNA cleaving ability of the complex (Fig. 8e, lane 6). Thus, it may be concluded that hydroxyl ion is associated with DNA cleavage exhibited by the complexes.

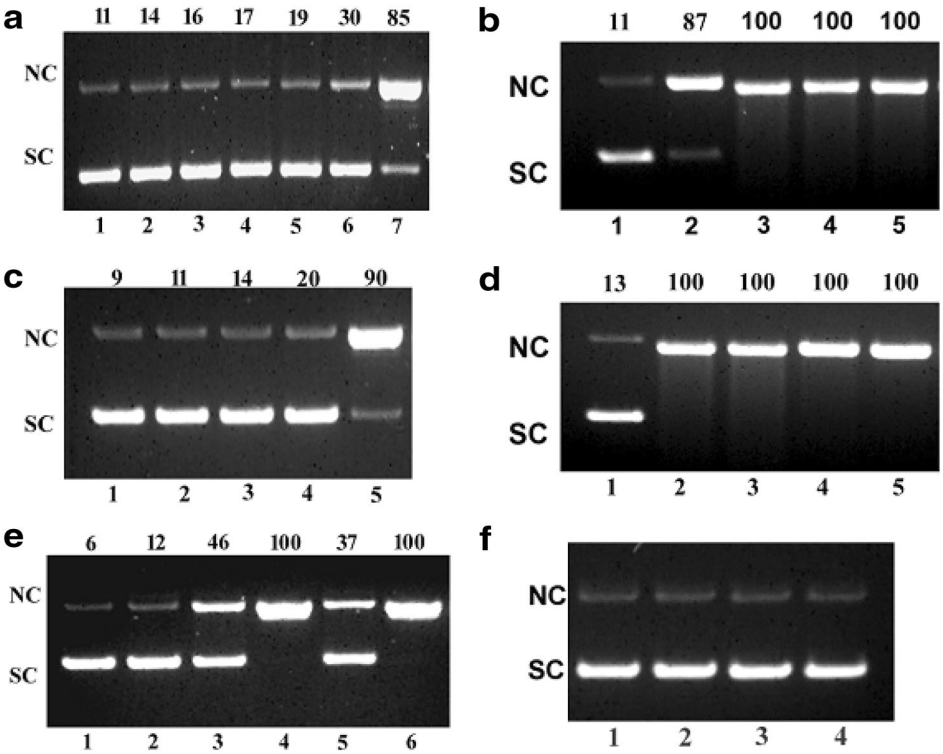

Fig. 8 Hydrolytic and oxidative cleavage of supercoiled *pUC19* DNA (200 ng) at 37 °C in 50 mM Tris–HCl buffer (pH 8.0). **a** Lane 1, DNA control; lane 2, DNA + **1** (5 μM); lane 3, DNA + **1** (10 μM); lane 4, DNA + **1** (20 μM); lane 5, DNA + **1** (30 μM); lane 6, DNA + **1** (40 μM); lane 7, DNA + **1** (50 μM). **b** Lane 1, DNA control; lane 2, DNA + **1** (50 μM); lane 3, DNA + **1** (100 μM); lane 4, DNA + **1** (150 μM); lane 5, DNA + **1** (200 μM). **c** Lane 1, DNA control; lane 2, DNA + **2** (5 μM); lane 3, DNA + **2** (10 μM); lane 4, DNA + **2** (20 μM); lane 5, DNA + **2** (30 μM). **d** Lane 1, DNA control; lane 2, DNA + **2** (50 μM); lane 3, DNA + **2** (100 μM); lane 4, DNA + **2** (150 μM); lane 5, DNA + **2** (200 μM). **e** Lane 1, DNA + H_2O_2 control; lane 2, DNA + **2** (5 μM) + H_2O_2; lane 3, DNA + **2** (15 μM) + H_2O_2; lane 4, DNA + **2** (25 μM) + H_2O_2; lane 5, DNA + **2** (25 μM) + H_2O_2 + DMSO (2 μL); lane 6, DNA + **2** (25 μM) + H_2O_2 + NaN_3 (100 μM). **f** Lane 1, control DNA; lane 2, DNA + $Cu(OAc)_2 \cdot 2H_2O$ (500 μM); lane 3, DNA + 1,5-bis(salicylidene)carbohydrazide (500 μM); lane 4, DNA + 1,10-phenanthroline monohydrate (500 μM)

To ensure that the copper complexes **1** and **2** as a whole are responsible for cleavage of DNA, control experiments were performed with $Cu(OAc)_2 \cdot H_2O$ (500 μM), free ligands 1,5-bis(salicylidene)carbohydrazide, (500 μM) and 1,10-phenanthroline monohydrate (500 μM). No cleavage was observed with either $Cu(OAc)_2 \cdot H_2O$, ligand 1,5-bis(salicylidene)carbohydrazide or coligand 1,10-phenanthroline monohydrate (Fig. 8f, lanes 2–4), even at a concentration of 500 μM. This confirms that neither $Cu(OAc)_2 \cdot H_2O$ nor the free ligands alone are capable of bringing about DNA strand cleavage.

Further, the kinetics of DNA cleavage were studied by monitoring the % DNA cleavage by the complexes **1** and **2** (200 μM) with time (Fig. 9). The time-dependent decrease of form I and increase of form II were found to fit well to a single-exponential decay and increase, respectively. A plot of log (% SC DNA) with time gave a linear fit from which the hydrolytic rate constant (k_{obs}) was obtained. The k_{obs} value obtained were 11.55 h^{-1} for **1** and 11.63 h^{-1} for **2**, respectively. This amounts to an enormous enhancement of cleavage rate of $3.21–3.23 \times 10^8$ in comparison to the unhydrolyzed rate of ds-DNA ($k = 3.6 \times 10^{-8}$ h^{-1}). This rate enhancement is much higher than the rate enhancements reported for most of the transition metal-based synthetic hydrolases [29, 30, 36, 45].

Cytotoxicity

Cell proliferation

The cytotoxicity of the complexes was tested against cells from A549 lung cancer cell line, MCF7 breast cancer cell line and HaCaT human keratinocyte normal cell line using the 3-(4,5-dimethylthiazol-2-yl)-2,5-diphenyltetrazolium bromide (MTT) assay. From the percentage cell viability versus complex concentration plot (Fig. 10), a dose-dependent cell death-inducing ability was observed for both the complexes **1** and **2**. It is observed that complex **1** exhibits more cytotoxicity than **2** in both A549 and MCF7cell

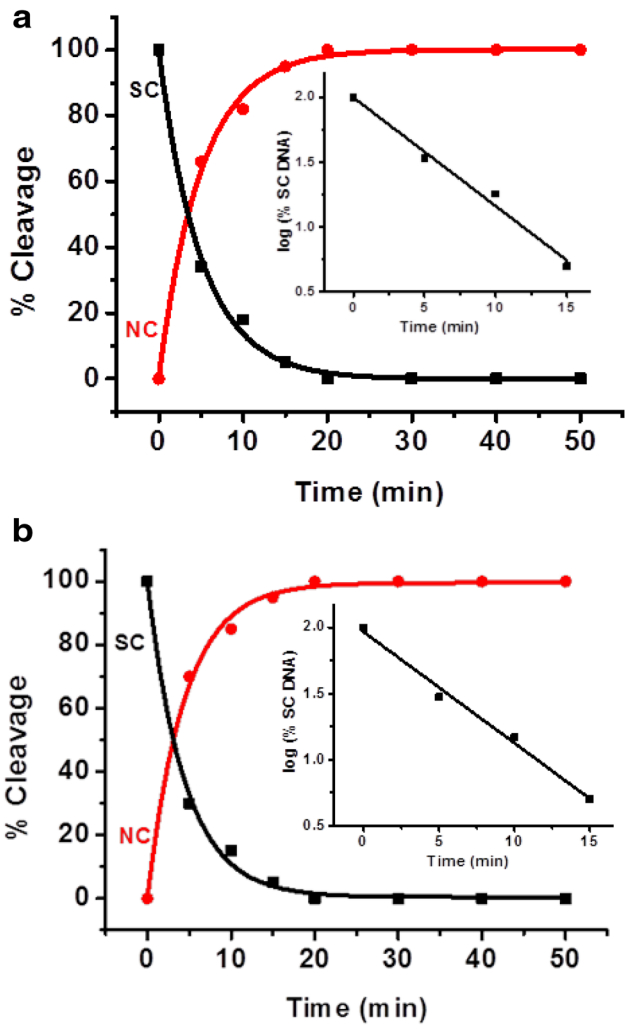

Fig. 9 Hydrolytic cleavage of SC *pUC19* DNA (200 ng) showing the decrease in form I (SC DNA) and the formation of form II (NC DNA) with the incubation time (in dark at 37 °C): **a** using 200 μM concentration of **1**; inset shows the plot of log(% SC DNA) vs. time for complex **1** (200 μM). **b** Using 200 μM concentration of **2**; inset shows the plot of log (% SC DNA) vs. time for complex **2** (200 μM)

lines. Most importantly, the complexes **1** and **2** appear to be comparatively less toxic to normal HaCaT cells (Fig. 10e, f). Especially in case of complex **2**, not much toxicity is observed till 5 μM dose in HaCaT cell line. At 10 μM concentration, **2** exhibited significant cytotoxicity as seen from cell viability of ~48% in both cancerous cell lines A549 and MCF7, whereas the cell viability was ~90% in normal HaCaT cell line; this marked difference between the cytotoxic effect in cancerous and noncancerous cell lines is of considerable importance. The IC_{50} values are presented in Table 2. The IC_{50} values for **1** and **2** for both A549 and MCF7 cell lines are found to be higher than that reported for cisplatin (4.13 μM for A549, 3.92 μM for MCF7). However, the IC_{50} values for **1** and **2** for MCF7 cell line are found to be much lower than that reported for carboplatin (36.65 μM for MCF7) [34]. Another point to be noted that though the results of DNA binding and cleavage studies exhibited by compounds **1** and **2** are very similar, their cytotoxic behavior toward A549, MCF7 and HaCaT cell lines are considerably different. This difference may originate from the difference in their abilities to diffuse across the cell membrane. Compound **1** being uncharged polar molecule will be able to passively diffuse across the cell membrane. On the other hand, compound **2** being ionic will find it difficult to diffuse across the cell membrane as compared to compound **1** [47]. Another point to be mentioned here is that the reported [41] neutral heterodinuclear Zn(II)/Cu(II) compound [Zn(*o*-phen)LCu(OAc)] (**3**) containing the enol form of the same carbohydrazone Schiff base (H_3L = *o*-$HOC_6H_4C(H)$=N–NH–C(OH)=N–N=C(H)-C_6H_4OH-*o*), which is structurally very similar to compound **1** under study, also exhibited [41] very high cytotoxicity against the human lung cancer A549 cell line (IC_{50} = 4.80 μM) and for the breast cancer MCF7 cell line (IC_{50} = 3.6 μM). At the same time, both these compounds **1** and **3** were found to be much less toxic at their 10 μM concentrations toward HaCaT normal cell line. On the other hand, compound **2**, which also contains Cu(II) in both the sites like compound **1**, but containing *o*-phen coligands in both the Cu(II) centers, exhibits relatively lesser cytotoxicity, in spite of containing two *o*-phen coligands in the molecule, not only toward both the cancer cells but also toward HaCaT normal cells as compared to compound **1** containing only one *o*-phen coligand in the first Cu(II) site and acetate in the second Cu(II) site.

We have also studied the cytotoxicity of the free ligands to compare that with their metal bound states in compounds **1** and **2**. The cytotoxicity study of the free Schiff base ligand and the free coligand 1,10-phenanthroline were carried out using the human lung cancer A549 cell line as a model case with different concentrations (0.5 μM, 1.0 μM, 2.5 μM, 5 μM, and 10 μM) of these free ligands for 24 h. The cell viabilities were found to be nearly 87% and 72% with 10 μM of the free Schiff base ligand and the free 1,10-phenanthroline ligand, respectively (Fig. S4, Supplementary material), suggesting that the free ligands are capable of causing individually about 13% and 28% cell death at 10 μM concentrations. On the other hand, the cell viabilities for the compounds **1** and **2** were found to be nearly 21% and 48% with 10 μM concentrations of **1** and **2**, respectively. Thus, copper chelation with these ligands certainly increased their toxicity, as observed for many other cases [1].

Very recently, we have reported [48] the cytotoxicity of a five-coordinate Cu(II) compound [Cu(pabt)(*o*-phen)](ClO_4) (**4**), (Hpabt = *N*-(2-mercaptophenyl)-2′-pyridylmethylenimine, *o*-phen = 1,10-phenanthroline) with A549 cell line and the IC_{50} value was found to be 5.26 μM, suggesting it is highly potent for the A549 cells. This

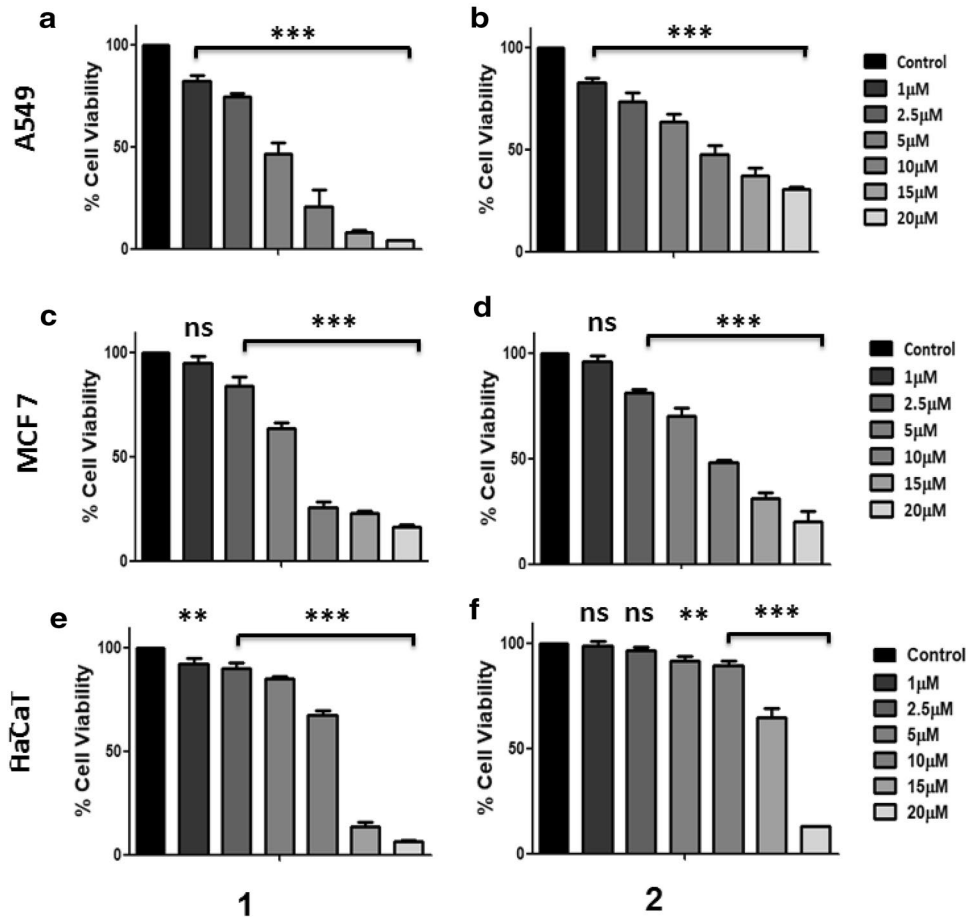

Fig. 10 Effect of **1** and **2** on cell viability in A549, MCF7 and HaCaT cell lines. Cells were treated with compounds **1** and **2** for 24 h. Effect of **1** and **2** on cell viability in **a**, **b** A549, **c**, **d** MCF7 and **e**, **f** HaCaT was analyzed by MTT assay. Data of three independent experiments are presented as mean ± SD. Difference in significance was determined by one-way ANOVA. $^{*}P < 0.05$, $^{**}P < 0.01$, $^{***}P < 0.001$, ns not significant

Table 2 IC_{50} values for the compounds **1** and **2** calculated from the plot of cell viability versus concentration in the MTT assay

Cell line	IC_{50} (μM)	
	Compd **1**	Compd **2**
A549	4.34	8.46
MCF 7	6.50	8.68
HaCaT	11.19	16.01

compound was found to be much less toxic toward the human keratinocyte HaCaT normal cells. Also, we have recently reported [49] the cytotoxicity of another five-coordinate [CuL(*o*-phen)] (**5**) and a four-coordinate [CuL(Imz)] (**6**), (H_2L = *o*-$HOC_6H_4C(H)=NC_6H_4OH$-*o*, *o*-phen = 1,10-phenanthroline, and Imz = imidazole) compounds with A549 and MCF7 cancer cell lines. Both these complexes were found to be very toxic for A549 cells (IC_{50} values were 0.67 and 0.59 μM, respectively) as well as quite toxic for MCF7 cells (IC_{50} values were 6.30 and 8.88 μM, respectively), but these two compounds were found to be equally toxic for HaCaT normal cells. Lu et al. [34] have studied the cytotoxicity of Cu(II) complexes, which also exhibited lower IC_{50} values in A549 as well as MCF7 cell lines, but the cytotoxic effect of these compounds on any normal cell line was not reported. Anjomshoa et al. [50] have studied the anticancer activity of a mononuclear Cu(II) complex with 5,6-diphenyl-3-(2-pyridyl)-1,2,4-triazine ligand and the reported IC_{50} values were 7.80 and 9.80 μM for A549 and MCF7 cells, respectively. Nair and coworkers [13] have studied the cytotoxic effects of two copper(II) complexes of terpyridine derivatives with human breast cancer MCF7 cell line and the IC_{50} values were found to be 6.25 and 3.125 μM for those two complexes. Abdi et al. [51] have reported the IC_{50} value for MCF7 cells (4.57 μM) of a mononuclear copper(II) complex with terpyridine and an extended phenanthroline base. Meenongwa et al. [52] have studied the effects of *N*,*N*-heterocyclic ligands on the in vitro cytotoxicity of some copper(II) chloride complexes with MCF7 cells, and a few of these compounds were found to be cytotoxic toward this cell line. Inspired by the first synthetic chemical nuclease, $[Cu(phen)_2]^{2+}$ (phen = 1,10-phenanthroline), and based on

Fig. 11 Apoptosis analysis by Annexin-V and propidium iodide staining. **a** A549 cells and **b** MCF7 cells treated with 1, 2.5, 5, 10, 15 and 20 μM of compounds **1** and **2** for 24 h. Effect on apoptosis was analyzed by Annexin-V/PI staining using flow cytometry. Representative data of three independent experiments are presented ▶

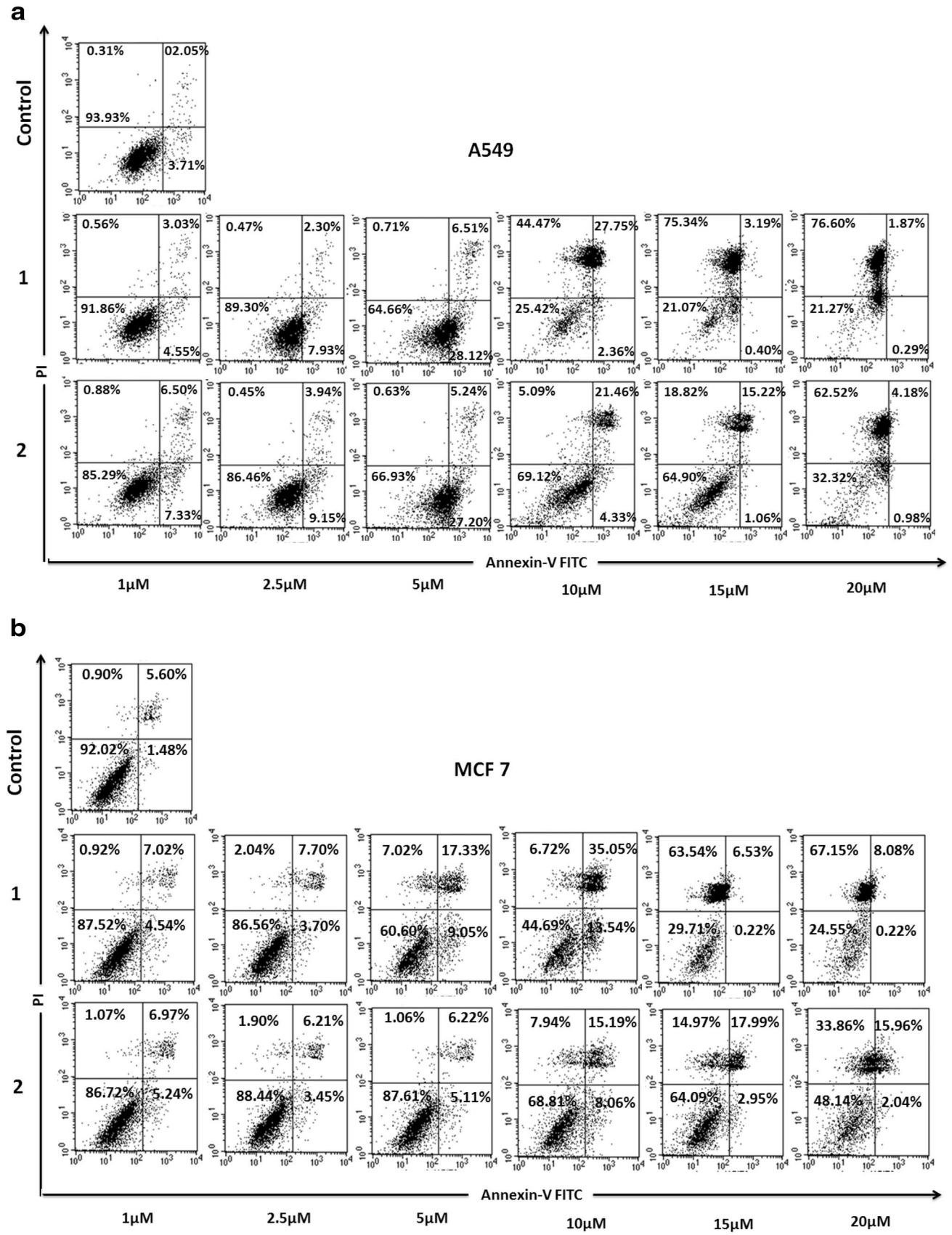
a
A549
Control
1
2
PI
Annexin-V FITC
0.31%
02.05%
93.93%
3.71%
0.56%
3.03%
91.86%
4.55%
0.47%
2.30%
89.30%
7.93%
0.71%
6.51%
64.66%
28.12%
44.47%
27.75%
25.42%
2.36%
75.34%
3.19%
21.07%
0.40%
76.60%
1.87%
21.27%
0.29%
0.88%
6.50%
85.29%
7.33%
0.45%
3.94%
86.46%
9.15%
0.63%
5.24%
66.93%
27.20%
5.09%
21.46%
69.12%
4.33%
18.82%
15.22%
64.90%
1.06%
62.52%
4.18%
32.32%
0.98%
1μM
2.5μM
5μM
10μM
15μM
20μM
b
MCF 7
Control
1
2
PI
Annexin-V FITC
0.90%
5.60%
92.02%
1.48%
0.92%
7.02%
87.52%
4.54%
2.04%
7.70%
86.56%
3.70%
7.02%
17.33%
60.60%
9.05%
6.72%
35.05%
44.69%
13.54%
63.54%
6.53%
29.71%
0.22%
67.15%
8.08%
24.55%
0.22%
1.07%
6.97%
86.72%
5.24%
1.90%
6.21%
88.44%
3.45%
1.06%
6.22%
87.61%
5.11%
7.94%
15.19%
68.81%
8.06%
14.97%
17.99%
64.09%
2.95%
33.86%
15.96%
48.14%
2.04%
1μM
2.5μM
5μM
10μM
15μM
20μM

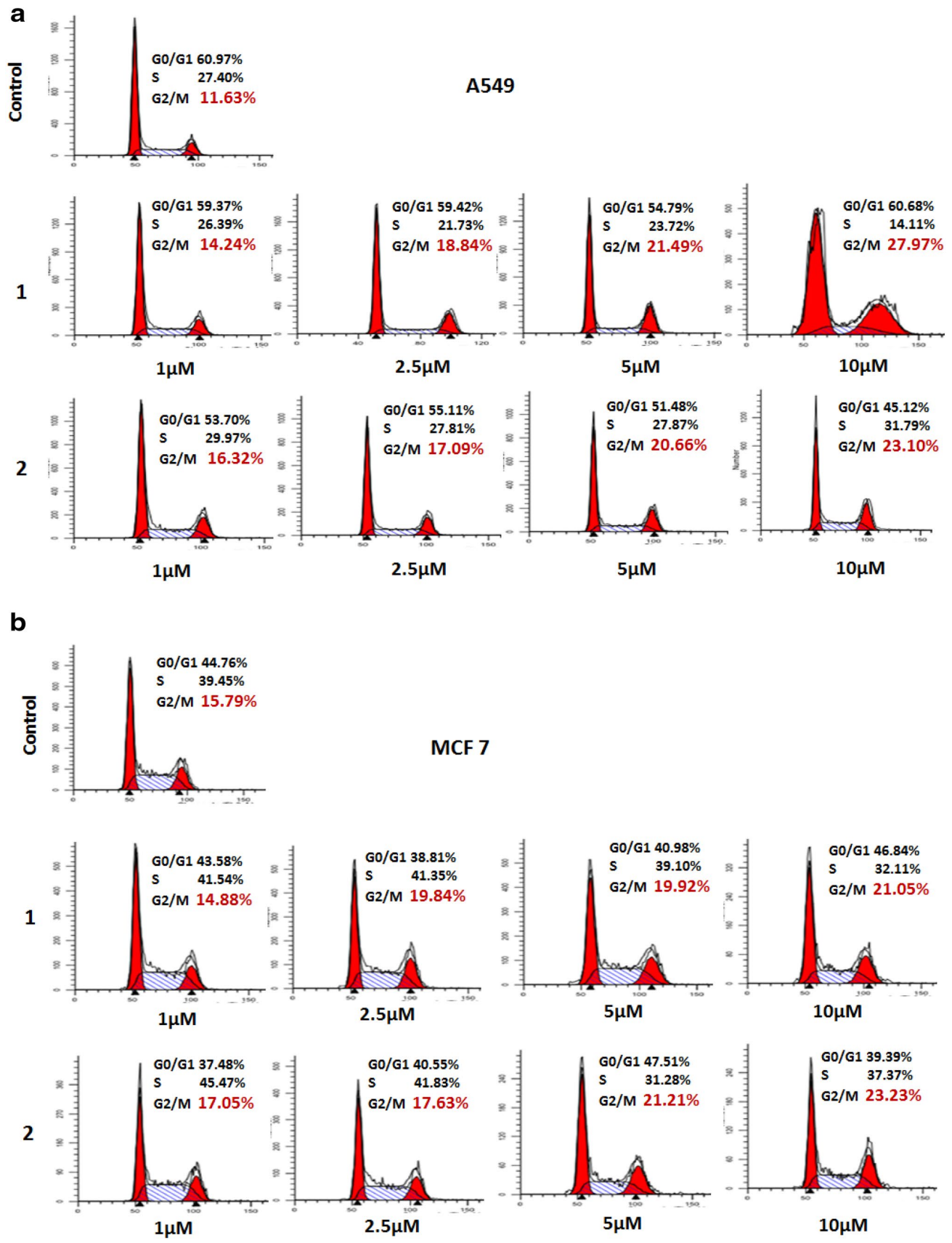
a
Control
G0/G1 60.97%
S 27.40%
G2/M 11.63%
A549
1
G0/G1 59.37%
S 26.39%
G2/M 14.24%
1μM
G0/G1 59.42%
S 21.73%
G2/M 18.84%
2.5μM
G0/G1 54.79%
S 23.72%
G2/M 21.49%
5μM
G0/G1 60.68%
S 14.11%
G2/M 27.97%
10μM
2
G0/G1 53.70%
S 29.97%
G2/M 16.32%
1μM
G0/G1 55.11%
S 27.81%
G2/M 17.09%
2.5μM
G0/G1 51.48%
S 27.87%
G2/M 20.66%
5μM
G0/G1 45.12%
S 31.79%
G2/M 23.10%
10μM
b
Control
G0/G1 44.76%
S 39.45%
G2/M 15.79%
MCF 7
1
G0/G1 43.58%
S 41.54%
G2/M 14.88%
1μM
G0/G1 38.81%
S 41.35%
G2/M 19.84%
2.5μM
G0/G1 40.98%
S 39.10%
G2/M 19.92%
5μM
G0/G1 46.84%
S 32.11%
G2/M 21.05%
10μM
2
G0/G1 37.48%
S 45.47%
G2/M 17.05%
1μM
G0/G1 40.55%
S 41.83%
G2/M 17.63%
2.5μM
G0/G1 47.51%
S 31.28%
G2/M 21.21%
5μM
G0/G1 39.39%
S 37.37%
G2/M 23.23%
10μM

◂**Fig. 12** Effects of **1** and **2** on cell cycle progression. **a** A549 and **b** MCF 7 cells treated with 1, 2.5, 5, 10, 15 and 20 μM of compounds **1** and **2** for 24 h. Effect on cell cycle arrest was analyzed by PI staining using flow cytometry. Representative data of three independent experiments are presented

the results that mononuclear [Cu(phen)$_2$(phthalate)] complexes exhibited very good chemotherapeutic potential against colon (HT29), breast (MCF7) and prostate (DU145) cancer cell lines, Kellett et al. [53] have synthesized and studied the water-soluble bis(1,10-phenanthroline) octanedioate Cu^{2+} (and Mn^{2+}) complexes that displayed extremely high cytotoxicity toward some human cancer cell lines (HT29, SW480 and SW620), but these were found to be less toxic toward normal human keratinocyte cells (HaCaT).

Copper(II) complexes with terpyridine ligands studied by Djuran and coworkers [54] exhibited very low IC_{50} values for A549 cells (1.2–1.9 μM). Apart from these there are studies [55–57] by Nair and coworkers involving A549 cell lines with Cu(II) complexes with imidazole terpyridine, with substituted terpyridine and terpyridine ligands and some of these complexes exhibited quite low IC_{50} values in A549 cells. Nagababu et al. [5] have studied the cytotoxicity of Cu complexes, two of which also exhibited low IC_{50} values in A549 cell line; however, these complexes were found to be cytotoxic also toward normal cell lines. Another study reported by Feng and Liu [58] for A549 cells with Cu(II)-complexes based on tricationic metalloporphyrin salicyloylhydrazone ligands, however, exhibited high IC_{50} values.

Annexin-V FITC/PI double staining study using flow cytometry

During the initial stages of apoptosis, the cells lose their membrane phospholipid asymmetry and the membrane phospholipid phosphatidylserine (PS) is translocated from the inner face of the plasma membrane to the cell surface. PS can be easily detected by staining with fluorescent conjugated Annexin-V that specifically binds to PS exposed to the cell surface, thereby allowing the detection of early apoptotic cells. Cells are stained in parallel with propidium iodide (PI) which can enter the cells only when the plasma membrane is damaged. Therefore, viable cells are Annexin-V and PI negative (Annexin-V−, PI−). Cells undergoing early apoptosis but having intact membranes exclude propidium iodide (PI); this allows us to distinguish between early apoptotic cells (Annexin-V+, PI−) from late apoptotic cells (Annexin-V+, PI+). Necrotic cells are Annexin negative and PI positive (Annexin-V−, PI+). To see the effect of the copper complexes under study, A549 and MCF7 cells were treated with the indicated doses of **1** and **2** (1 μM, 2.5 μM, 5 μM, 10 μM, 15 μM and 20 μM) for 24 h and the percentage cell death was analyzed by Annexin-V FITC/PI staining using flow cytometry. Our results showed drastic decrease in viable cells (lower left quadrant Annexin-V−, PI−) in a dose-dependent manner upon treatment with **1** and **2** as compared to that of control cells in both A549 (Fig. 11a) and MCF7 (Fig. 11b) cell lines studied.

It is observed that A549 cells upon incubation for 24 h with each of the complexes **1** and **2** show a general trend of increase in early apoptotic cells with increasing complex concentration up to 5 μM (lower right quadrant: Annexin-V+, PI−). Then a large population of late apoptotic cells 27.75% and 21.46% (upper right quadrant) corresponding to treatment of 10 μM concentration of **1** and **2** was observed. Also, it is noted that from 10 μM dose onward, there is a steady decrease in cell population in the lower right quadrant as most of the cells have passed onto the late apoptotic/necrotic stage from early apoptotic stage (Fig. 11b).

In case of MCF7 cell line upon incubation with each of the complexes **1** and **2** for 24 h, a general trend of increase in early apoptotic cells with increasing complex concentration up to 10 μM (lower right quadrant: Annexin-V+, PI−) is seen. Also a higher population of late apoptotic cells (35.05%) is observed in case of 10 μM dose of **1** (upper right quadrant) as compared to 15.19% cell population upon treatment with the same dose of **2**; this observation is in good agreement with that observed in the MTT assay (Fig. 10c, d). On further increasing the complex concentration to 15 and 20 μM, there is steady decrease in the cell population in the lower right quadrant which represents early apoptotic cells, as they may have passed onto next stage (late apoptosis/necrosis) (Fig. 11b).

Cell cycle analysis

The progression of cells through the different phases of cell cycle is controlled by check points at different stages. Most of the anti-proliferative drugs target distinct points in the cell cycle and control cell cycle phase progression [46, 59, 60]. Experiments were carried out to determine the phase of the cell cycle in which the compounds **1** and **2** arrested the cell growth. A549 and MCF7 cells were synchronized by serum starvation for 12 h, and after serum starvation A549 and MCF7 cells were grown in DMEM media and treated with 1, 2.5, 5 and 10 μM concentrations of **1** and **2** for 24 h. The DNA content of cells was determined by flow cytometry after the cells were stained with propidium iodide (PI). In case of both compounds, the results showed considerable increase in the G2/M phase in both cell lines in a dose-dependent manner (Fig. 12). As seen for the A549 cell line (Fig. 12a), the cell population increased up to 27.97% and 23.10% upon treatment with 10 μM dose of **1** and **2**, respectively, as compared to 11.63% cell population in G2/M of control. Similarly, for MCF7 cell line, the cell population increased up to 21.05% and 23.23% upon treatment with

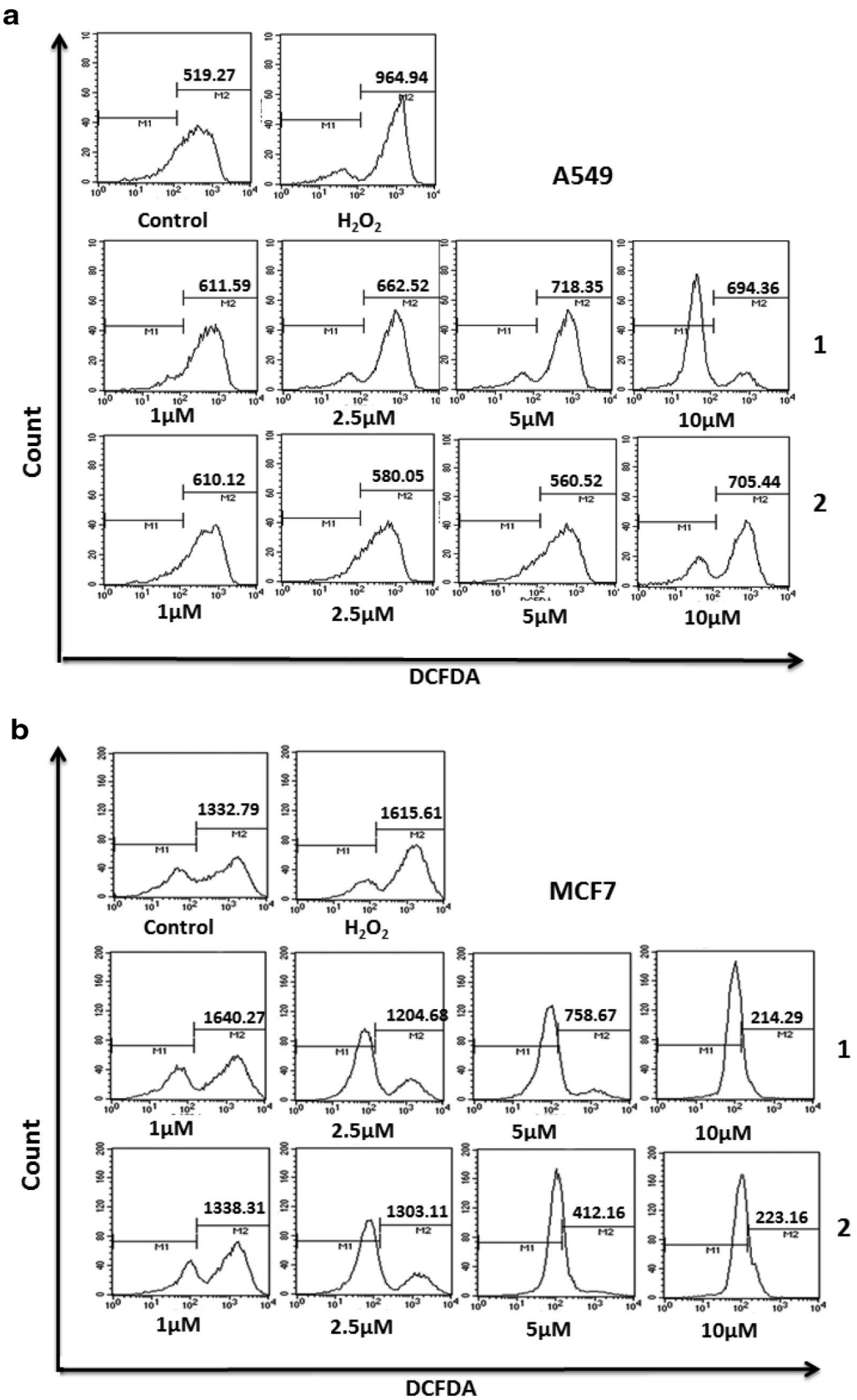
a
519.27
964.94
A549
Control
H_2O_2
611.59
662.52
718.35
694.36
1
1μM
2.5μM
5μM
10μM
610.12
580.05
560.52
705.44
2
1μM
2.5μM
5μM
10μM
Count
DCFDA
b
1332.79
1615.61
MCF7
Control
H_2O_2
1640.27
1204.68
758.67
214.29
1
1μM
2.5μM
5μM
10μM
1338.31
1303.11
412.16
223.16
2
1μM
2.5μM
5μM
10μM
Count
DCFDA

◂**Fig. 13** Effects of **1** and **2** on cellular ROS generation. **a** A549 and **b** MCF 7 cells treated with 1, 2.5, 5, 10, 15 and 20 μM of compounds **1** and **2** for 24 h. Effect on cellular ROS generation was analyzed by DCFDA staining using flow cytometry. Representative data of three independent experiments are presented

10 μM dose of **1** and **2**, respectively, as compared, to 15.79% cell population in the G2/M of control (Fig. 12b). DNA damage is known to be a key factor that triggers cell cycle arrest. Nuclease activity studied by gel electrophoresis experiments indicate that both **1** and **2** are highly capable of inducing hydrolytic as well as oxidative DNA cleavage (Fig. 8). Thus, extensive DNA damage caused by the treatment of **1** and **2** may have resulted in the G2/M phase arrest [45, 61, 62] in A549 and MCF7 cells.

Effect of compounds 1 and 2 on cellular ROS generation

To assess the capability of the complexes **1** and **2** to generate intracellular reactive oxygen species (ROS), A549 and MCF7 cells were treated with 1, 2.5, 5 and 10 μM concentrations of **1** and **2** for 24 h and the intracellular ROS levels were determined by flow cytometry using the redox-sensitive fluorescent probe 2′,7′ dichlorodihydrofluorescein diacetate (H_2DCFDA). It was observed that in A549 cell line, there was considerable ROS generation upon treatment with **1** and **2**. As indicated by the results at 10 μM concentration of **1** and **2**, ROS detected (694.36, 705.44) was considerably high compared to untreated A549 cells (519.27) (Fig. 13a), but not so significantly high to account for the total cytotoxicity observed from their MTT assay. These observations suggest that increased ROS level may be one of the factors responsible for the observed apoptosis in A549 cells. However, in MCF7 cells we observed that **1** and **2** decreased ROS level in a dose-dependent manner and that the ROS level was drastically decreased from 1332.79 (control) to 214.29 and 223.16 upon treatment with 10 μM dose of **1** and **2**, respectively (Fig. 13b), which is intriguing. There are reports that not only the increased ROS level, but also the depletion of ROS below a certain threshold level may lead to cancer cell killing [63, 64]. Liou and Storz [64] have discussed elaborately the role of reactive oxygen species (ROS) in cancer. They have pointed out that though the role for ROS-activated Erk1/2 (extracellular regulated kinase 1/2) signaling in cell proliferation is well known [65–67], its ability to regulate cancer cell survival appears to be very specific for cell type [68–70]. As an example, they have mentioned that when MCF-7 and MDA-MB-435 breast cancer cells were treated with ROS scavengers or inhibitors that target Erk1/2 or its upstream kinase MEK (mitogen-activated protein kinase kinase), it resulted in apoptosis and cell adhesion [71, 72]. Thus, the decrease in ROS levels by **1** and **2** in MCF7 cells in the present study is not surprising and may be associated with observed apoptosis. However, it is important to note that both the compounds **1** and **2** show G2/M phase cell cycle arrest in both A549 and MCF7 cell lines and activate ROS level in A549 cell line, but they act as scavengers or inhibitors of ROS in MCF7 cell line as analyzed by DCFDA staining using flow cytometry.

Conclusions

Two homodinuclear mixed ligand copper(II) complexes were structurally characterized by X-ray crystallography and their biological activities studied under identical experimental conditions. The compounds efficiently bind to CT-DNA with intercalative binding mode that is supported by viscosity measurements as well as from the fluorescence spectroscopic studies of ethidium bromide displacement assay. Both the compounds exhibit efficient hydrolytic DNA cleavage of SC *pUC19* DNA and the k_{obs} values were found to be 11.55 h^{-1} for **1** and 11.63 h^{-1} for **2**, respectively. This amounts to an enormous enhancement of cleavage rate of $3.21–3.23 \times 10^8$ in comparison to the unhydrolyzed rate of ds-DNA ($k = 3.6 \times 10^{-8}$ h^{-1}). Though both these compounds exhibit strong in vitro cytotoxicity against human lung cancer A549 cell line and human breast cancer MCF7 cell line as evident from significant decrease in cell viability and are found to be potent for both these cell lines as revealed from their IC_{50} values, compound **2**, in spite of containing *o*-phen coligands in both the Cu(II) sites, exhibits relatively lesser cytotoxicity not only toward both the cancer cells, but also toward HaCaT normal cells as compared to compound **1** containing only one *o*-phen coligand in the first Cu(II) site and acetate in the second Cu(II) site. This difference may be attributed to the difference in their abilities to diffuse across the cell membrane. Annexin-V/PI dual staining results analyzed by flow cytometry strongly suggest the induction of the apoptotic pathway for the anticancer activity of these complexes. Cell cycle analysis with compounds **1** and **2** showed cell cycle arrest in the G2/M phase in both A549 and MCF7 cell lines. However, the most important observation made in this study is that compounds **1** and **2** showed differential behavior toward ROS in these two cancer cell lines. While both of them were found to be activators of ROS in A549 cells, they acted as inhibitors or scavengers of ROS in MCF7 cells.

Acknowledgements We thank the SAIF, IIT-Madras, for XRD and SAIF, IIT-Bombay, for EPR facilities. A.P.K. thanks Mr. Atanu Banerjee and Prof. Rupam Dinda, Department of Chemistry, National Institute of Technology, Rourkela, India, for help with the ESI-MS results. MK thanks SERB, DST, Government of India, for the Project EMR/2017/001562.

References

1. Santini C, Pellei M, Gandin V, Porchia M, Tisato F, Marzano C (2014) Chem Rev 114:815–862
2. Barone G, Terenzi A, Lauria A, Almerico AM, Leal JM, Busto N, García B (2013) Coord Chem Rev 257:2848–2862 **(and references therein)**
3. Todd RC, Lippard SJ (2009) Metallomics 1:280–291
4. Zhang CX, Lippard SJ (2003) Curr Opin Chem Biol 7:481–489
5. Nagababu P, Barui AK, Thulasiram B, Shobha Devi C, Satyanarayana S, Patra CR, Sreedhar B (2015) J Med Chem 58:5226–5241
6. Adak P, Ghosh B, Bauza A, Frontera A, Blake AJ, Corbella CM, Das-Mukhopadhyay C, Chattopadhyay SK (2016) RSC Adv 6:86851–86861
7. Chauhan M, Banerjee K, Arjmand F (2007) Inorg Chem 46:3072–3082
8. Vijayalakshmi R, Kanthimathi M, Parthasarathi R, Nair BU (2006) Bioorg Med Chem 14:3300–3306
9. Walker MG, Gonzalez V, Chekmeneva E, Thomas JA (2012) Angew Chem Int Ed 51:12107–12110
10. Fabbro C, Ali-Boucetta H, Ros TD, Kostarelos K, Bianco A, Prato M (2012) Chem Commun 48:3911–3926
11. Farrer NJ, Salassa L, Sadler PJ (2009) Dalton Trans 10690–10701
12. Rajalakshmi S, Kiran MS, Nair BU (2014) Eur J Med Chem 80:393–406
13. Rajalakshmi S, Weyhermuller T, Dinesh M, Nair BU (2012) J Inorg Biochem 117:48–59
14. Basu U, Khan I, Hussain A, Kondaiah P, Chakravarty AR (2012) Angew Chem Int Ed 51:2658–2661
15. Basu U, Khan I, Koley D, Saha S, Kondaiah P, Chakravarty AR (2012) J Inorg Biochem 116:77–87
16. Goswami TK, Gadadhar S, Roy M, Nethaji M, Karande AA, Chakravarty AR (2012) Organometallics 31:3010–3021
17. Goswami TK, Chakravarthi BVSK, Roy M, Karande AA, Chakravarty AR (2011) Inorg Chem 50:8452–8464
18. Devereux M, Shea DO, Kellett A, McCann M, Walsh M, Egan D, Deegan C, Kedziora K, Rosair G, Muller-Bunz H (2007) J Inorg Biochem 101:881–892
19. O'Connor M, Kellett A, McCann M, Rosair G, McNamara M, Howe O, Creaven BS, McClean S, Foltyn-Arfa Kia A, O'Shea D, Devereux M (2012) J Med Chem 55:1957–1968
20. Tardio S, Basanetti I, Bignardi C, Elviri L, Tegoni M, Mucchino C, Bussolati O, Franchi-Gazzola R, Marchio L (2011) J Am Chem Soc 133:6235–6242
21. Dey D, Kaur G, Ranjani A, Gayathri L, Chakraborty P, Adhikary J, Pasan J, Dhanasekaran D, Choudhury AR, Akbarsha MA, Kole N, Biswas B (2014) Eur J Inorg Chem 3350–3358
22. Festa RA, Thiele DJ (2011) Curr Biol 21:877–883
23. Parveen S, Tabassum S, Arjmand F (2017) RSC Adv 7:6587–6597
24. Liu J, Zhang T, Lu T, Qu L, Zhou H, Zhang Q, Ji L (2002) J Inorg Biochem 91:269–276
25. Selvakumar B, Rajendiran V, Uma Maheswari P, Stoeckli-Evans H, Palaniandavar M (2006) J Inorg Biochem 100(3):316–330
26. Mal SK, Mitra M, Kaur G, Manikandamathavan VM, Kiran MS, Roy Choudhury A, Unni Nair B, Ghosh R (2014) RSC Adv 4:61337–61342
27. Saswati Chakroborty A, Dash SP, Panda AK, Acharyya R, Biswas A, Mukhopadhyay S, Bhutia SK, Crochet A, Patil YP, Nethaji M, Dinda R (2015) Dalton Trans 44:6140–6157
28. Kumaravel G, Utthra PP, Raman N (2018) Bioorg Chem 77:269–279
29. Burstyn JN, Deal KA (1993) Inorg Chem 32:3585–3586
30. Deal KA, Hengge AC, Burstyn JN (1996) J Am Chem Soc 118:1713–1718
31. Itoh T, Hisada H, Sumiya T, Hosono M, Usui Y, Fujii Y (1997) Chem Commun 677–678
32. Sissi C, Mancin F, Gatos M, Palumbo M, Tecilla P, Tonellato U (2005) Inorg Chem 44(7):2310–2317
33. Wang J, Xia Q, Zheng X, Chen H, Chao H, Mao Z, Ji L (2010) Dalton Trans 39:2128–2136
34. Lu J, Sun Q, Li JL, Jiang L, Gu W, Liu X, Tian JL, Yan SP (2014) J Inorg Biochem 137:46–56
35. Li F, Xie J, Feng F (2015) New J Chem 39:5654–5660
36. Reddy PAN, Nethaji M, Chakravarty AR (2004) Eur J Inorg Chem 1440–1446
37. Dhar S, Reddy PAN, Chakravarty AR (2004) Dalton Trans 697–698
38. Ramakrishnan S, Rajendiran V, Palaniandavar M, Periasamy VS, Srinag BS, Krishnamurthy H, Akbarsha MA (2009) Inorg Chem 48:1309–1322
39. Reddy PR, Silpa A (2011) Polyhedron 30:565–572
40. Reddy PR, Silpa A (2011) Chem Biodivers 8:1245–1265
41. Koley MK, Duraipandy N, Kiran MS, Varghese B, Manoharan PT, Koley AP (2017) Inorg Chim Acta 466:538–550
42. Bruker I (2016) Apex3 v2017.3-0, SAINT V8.38A, Bruker AXS Inc.: Madison (WI), USA, 2013/2014
43. Sheldrick GM (2014). SHELXL version 2014. University of Göttingen, Germany
44. Frrugia LJ (1997) J Appl Cryst 30:565–566
45. Parsekar SU, Fernandes J, Banerjee A, Chouhan Om P, Biswas S, Singh M, Mishra DP, Kumar M (2018) J Biol Inorg Chem 23:1331–1349
46. Rastogi N, Duggal S, Singh SK, Porwal K, Srivastava VK, Maurya R, Bhatt ML, Mishra DP (2015) Oncotarget 6:43310–43325
47. Nicole JY, Marlon JH (2015) Methods Mol Biol 1266:29–53
48. Kumar M, Parsekar SU, Duraipandy N, Kiran MS, Koley AP (2019) Inorg Chim Acta 484:219–226
49. Kumar M, Parsekar SU, Duraipandy N, Kiran MS, Varghese B, Manoharan PT, Koley AP (2018) Inorg Chim Acta 478:211–221
50. Anjomshoa M, Hadadzadeh H, Torkzadeh-Mahani M, Fatemi SJ, Adeli-Sardou M, Rudbari HA, Nardo VM (2015) Eur J Med Chem 96:66–82
51. Abdi K, Hadadzadeh H, Weil M, Salimi M (2012) Polyhedron 31:638–648
52. Meenongwa A, Brissos RF, Soikum C, Chaveerach P, Gamez P, Trongpaniche Y, Chaveerach U (2016) New J Chem 40:5861–5876
53. Kellett A, O'Connor M, McCann M, Howe O, Casey A, McCarron P, Kavanagh K, McNamara M, Kennedy S, May DD, Skell PS, O'Shea D, Devereux M (2011) Med Chem Commun 2:579–584
54. Glišic BD, Nikodinovic-Runic J, Ilic-Tomic T, Wadepohl H, Veselinovic A, Opsenica IM, Djuran MI (2018) Polyhedron 139:313–322
55. Manikandamathavan VM, Nair BU (2013) Eur J Med Chem 68:244–252
56. Rajalakshmi S, Weyhermller T, Freddy AJ, Vasanthi HR, Nair BU (2011) Eur J Med Chem 46:608–617
57. Manikandamathavan VM, Rajapandian V, Freddy AJ, Weyhermuller T, Subramanian V, Nair BU (2012) Eur J Med Chem 57:449–458
58. Feng X, Liu J (2018) J Inorg Biochem 178:1–8
59. Senderowicz AM, Sausville EA (2000) J Natl Cancer Inst 92:376–387
60. Jackson JR, Gilmartin A, Imburgia C, Winkler JD, Marshall LA, Roshak A (2000) Can Res 60:566–572
61. DiPaola RS (2002) Clin Cancer Res 8:3512–3519
62. Tyagi AK, Singh RP, Agarwal C, Chan DC, Agarwal R (2002) Clin Cancer Res 8:3512–3519
63. Wang J, Yi J (2008) Cancer Biol Ther 7:1875–1884
64. Liou G-Y, Storz P (2010) Free Radic Res 44:479–496

65. Irani K, Xia Y, Zweier JL, Sollott SJ, Der CJ, Fearon ER, Sundaresan M, Finkel T, Goldschmidt-Clermont PJ (1997) Science 275:1649–1652
66. McCubrey JA, Steelman LS, Chappell WH, Abrams SL, Wong EW, Chang F, Lehmann B, Terrian DM, Milella M, Tafuri A, Stivala F, Libra M, Basecke J, Evangelisti C, Martelli AM, Franklin RA (2007) Biochim Biophys Acta 1773:1263–1284
67. Kumar B, Koul S, Khandrika L, Meacham RB, Koul HK (2008) Cancer Res 68:1777–1785
68. Chan DW, Liu VW, Tsao GS, Yao KM, Furukawa T, Chan KK, Ngan HY (2008) Carcinogenesis 29:1742–1750
69. Lee WC, Choi CH, Cha SH, Oh HL, Kim- YK (2005) Neurochem Res 30:263–270
70. Rygiel TP, Mertens AE, Strumane K, van der Kammen R, Collard JG (2008) J Cell Sci 121:1183–1192
71. Ostrakhovitch EA, Cherian MG (2005) J Cell Biochem 95:1120–1134
72. Zhou J, Chen Y, Lang J-Y, Lu J-J, Ding J (2008) Mol Cancer Res 6:194–204